

Comet Explorers - Space Mission Design Proposal

Guerrero Hernández, Aníbal

Chair of Pico and Nano Satellites (PNS)

Technical University of Munich (TUM)

Munich, Germany

anibal.guerrero@tum.de

Frühholz Eitner, Leonardo

Tinucci, Alessandro

Chair of Pico and Nano Satellites (PNS)

Technical University of Munich (TUM)

Munich, Germany

leonardo.eitner@tum.de

Munich, Germany

at.tinucci@tum.de

Thepdawala, Sibtain Ali

Chair of Pico and Nano Satellites (PNS)

Technical University of Munich (TUM)

Munich, Germany

sibtainali.thepdawala@tum.de

CONTENTS

I	Introduction	4	V-B	ADCS [Sibtain Ali]	17
	I-A Background Information	4		V-B1 Attitude Dynamics	17
	I-B Relevance in the Current Landscape of the Space Industry	4		V-B2 Sensors	17
				V-B3 Actuators	18
				V-B4 Control Algorithms and Simulation	19
II	Mission Statement & Objectives [Sibtain Ali]	5	V-C	On-Board Computers & Software [Sibtain Ali]	21
	II-A Primary Objective	5		V-C1 Software Architecture	22
	II-B Secondary Objectives	5		V-C2 Data Processing Algorithms	22
	II-C Requirements	5		V-C3 Data Storage Strategy	22
	II-D Expected Deliverables from the Mission	5	V-D	Structural Design [Leo Eitner]	23
				V-D1 Materials	23
III	Simulation Framework [Alessandro Tinucci]	6		V-D2 Mechanisms	23
	III-A GMATLAB	6		V-D3 Launcher Compatibility	24
IV	Mission Analysis & Design	7		V-D4 Mass and Volume Budget	24
	IV-A Comet Selection [Leo Eitner]	7	V-E	Propulsion Subsystem [Leo Eitner]	24
	IV-B Concept of Operations [Anibal Guerrero]	7		V-E1 Electrical Propulsion	24
	IV-C Orbit Design [Alessandro Tinucci]	7		V-E2 First trade-off	25
	IV-C1 Earth Orbit	8		V-E3 Second Trade-Off	25
	IV-C2 Interplanetary Orbit	8	V-F	Power System [Anibal Guerrero]	26
	IV-C3 Comet Orbit	10		V-F1 Power Budget	26
	IV-D Payload Strategy	10		V-F2 Trade-Off & Requirements	26
	IV-D1 Observation [Leo Eitner]	10		V-F3 Solar Arrays	27
	IV-D2 Mining [Anibal Guerrero]	11		V-F4 Battery	28
	IV-D3 Comet 324P Chemical Composition [Anibal Guerrero]	11		V-F5 Final Characteristics	28
	IV-D4 Example Use Case [Anibal Guerrero]	12	V-G	Thermal Control [Alessandro Tinucci]	29
	IV-D5 Use Case Calculations [Anibal Guerrero]	13	VI	Payload Integration	31
	IV-E Payload Use Case - Surface Flatness [Alessandro Tinucci]	13	VI-A	Mechanical Integration [Leo Eitner]	31
V	Spacecraft System Design	16		VI-A1 Optical Payload	31
	V-A Communication System [Leo Eitner]	16		VI-A2 Rover	31
	V-A1 Science data	16	VI-B	Electrical Integration [Anibal Guerrero]	31
	V-A2 TT&C	16		VI-C Software Integration [Sibtain Ali]	32
			VII	Launch & Deployment	33
			VII-A	Launch Strategy [Anibal Guerrero]	33
			VII-B	Deployment Sequence [Leo Eitner]	33

		LIST OF TABLES
VIII	Mission Operations [Leo Eitner]	34
VIII-A	Ground Station Design	34
VIII-B	Communication Windows	34
VIII-C	Expected Data Volume	34
IX	Risk Management	35
IX-A	Risk Analysis, Mitigation and Backup [Sibtain Ali]	35
IX-B	Budget & Cost Analysis [Anibal Guerrero]	37
IX-B1	Launch Costs	37
IX-B2	Operational Costs	37
IX-B3	Development Costs	38
IX-B4	Total Cost Estimation	38
X	Timeline [Anibal Guerrero]	40
XI	End-of-life Planning	41
XI-A	Expected Mission Life [Anibal Guerrero]	41
XI-B	Deorbiting Strategies [Alessandro Tinucci]	41
XII	Conclusions [Everyone]	42
XIII	APPENDIX	43
XIII-A	Subsystem Level Requirements	43
XIII-B	ADCS Subsystem	44
XIII-C	Power Subsystem	45
References		46
I	High-Level Requirements	5
II	Initial Orbit Parameters	8
III	Interplanetary Burn Parameters	9
IV	IR camera specifications	11
V	Key Technical Parameters of RASSOR	12
VI	Components in Approximate Weight Percentage, Method of Analysis, Origin, and Mixing Ratio Range expected to be found in Comet 324P/La Sagra	13
VII	Efficiencies of all Processes Involved	13
VIII	Calculations of Masses and Trips Required for Theoretical Use Case	13
IX	RASSOR Requirements and Mission Information	14
X	Ka-band link budget and achieved bit rate.	16
XI	X-band link budgets.	17
XII	Sensors and their standout performance parameters	18
XIII	Actuators and their standout performance parameters	18
XIV	On-Board Computer Specifications	22
XV	Mass Budget	24
XVI	Simplified Volume Budget	24
XVII	Types of propellant	25
XVIII	Criteria and Weights	25
XIX	First trade-off results.	25
XX	Criteria and Weights	26
XXI	Second trade-off results.	26
XXII	Total propellant required.	26
XXIII	Power Budget	27
XXIV	Solar Cell Efficiency	27
XXV	Final Battery & Solar Array Characteristics	28
XXVI	Technical Information on Launch Opportunity.	33
XXVII	Expected Data Rates	34
XXVIII	Risks Analysis, Mitigation and Backup	35
XXIX	Launch Cost Calculations	37
XXX	Operational Costs Breakdown using the Deep Space Network, assuming a connection 3 days per week.	38
XXXI	Development Costs for Analogous Missions & Average	38
XXXII	Total Costs of the Mission	38
XXXIII	Most Common Spacecraft Power Sources Comparison	45

LIST OF FIGURES

1	GMATLAB Functional Diagram	6
2	<i>Comet Explorer's</i> Concept of Operations.	7
3	Earth - LaSagra Numerical Porkchop Plot	9
4	Interplanetary orbit algorithm progress in GMAT.	9
5	Final transfer orbit analysis values.	10
6	Optical payload design diagram.	10
7	RASSOR: Regolith Advanced Surface Systems Operations Robot	11
8	RASSOR excavating a slot trench in BP-1.	12
9	Mass Degradation through O_2 extraction process from original regolith collected by RASSOR.	14
10	Individual time required per RASSOR activity, and overall mining time.	14
11	3D Scanned view of a sample comet.	14
12	2D Analysis of landing zone.	15
13	Orbit analysis through area coverage.	15
14	Arbitrary satellite showing thruster configuration	18
15	Simulation Scheme	19
16	Angular velocity variation	20
17	Euler Angles variation	20
18	Thrust Output	20
19	Control Torque variation	20
20	Angular velocity variation	20
21	Euler Angles variation	21
22	Pointing Error	21
23	Thrust Output	21
24	Control Torque	21
25	Pointing Error	21
26	Thrust Output (Impulses)	21
27	On-board Computer: SpaceCloud iX10-101A [22]	22
28	Use Case Example of the selected on-board computer	22
29	Satellite airframe.	23
30	Main module deployed.	23
31	Ore retriever deployed.	24
32	Solar array dimensions, as provided by DHV [5].	28
33	Representation of 3 unfolded solar arrays, as provided by DHV [5].	28
34	ibeos B28-1100 Satellite Battery [20].	29
35	Spacecraft's thermal model in Simscape.	29
36	Spacecraft's temperature fluctuations.	29
37	SpaceX's Starship mounted to their launch tower at Starbase, TX.	33
38	Communication outages diagram.	34
39	Time Management for design concept of this mission, subdivided in objectives and tasks.	40
40	ClickUp Task assignation example for <i>Comet Explorers</i> ' mission.	40
41	Subsystem Level Requirements	43
42	Subsystem Level Requirements Continued	43
43	Simulink Framework for pointing	44
44	Simulink Framework for detumbling	44
45	Reference disturbance torques in the asteroid belt at 1.8 AU for different satellite orbits	44

Abstract—The Comet Explorers mission proposal aims to explore and exploit the resources of Main-Belt Comets (MBCs) utilizing SpaceX's Starship platform. The mission represents a pioneering endeavor aimed at exploring and exploiting the resources of Main-Belt Comets (MBCs) in the asteroid belt. With the aim of retrieving samples of volatile materials, such as water ice and organic compounds, and bringing them back to Earth, the mission seeks to advance scientific understanding of planetary formation and the origins of Earth's water and demonstrate advanced mining technology in the process. Owing to the reduced cost of the mission offered by SpaceX in the future, a preliminary design study is conducted to determine the technical feasibility of such a mission. The challenges of reduced gravitational forces in small bodies of the asteroid belt such as Main Belt Comets (MBCs) and the optimization of interplanetary trajectory will be touched upon, with details following for the spacecraft subsystems to identify and evaluate the technology readiness level of components compatible for such a mission. By addressing identified challenges and refining mission parameters, the scientific return of the mission can be maximized to achieve groundbreaking discoveries in planetary science, as well as the identification of more MBCs for future missions. [Sibtain Ali]

Index Terms—asteroid mining, asteroids, comets, RASSOR, space mission design

I. INTRODUCTION

A. Background Information

The Main-Belt Comet Mining Mission represents a ground-breaking endeavor aimed at unlocking the potential of Main-Belt Comets (MBCs) in the asteroid belt. These comets are believed to harbor valuable resources, including water ice and organic compounds, which hold significant implications for understanding the origins of Earth's water and supporting future space exploration endeavors. The mission is driven by the need to address fundamental questions in planetary science and advance our understanding of solar system dynamics. Additionally, the successful extraction and utilization of resources from MBCs could pave the way for sustainable space exploration and colonization efforts, offering new opportunities for scientific research, technological innovation, and economic development in space.

B. Relevance in the Current Landscape of the Space Industry

The mission under consideration can prove to be a major milestone for the space industry because of the following reasons:

- **Resource Utilization:** As space agencies and commercial entities increasingly look towards long-duration space missions and exploration beyond Earth orbit, the ability to extract and utilize resources from celestial bodies becomes paramount. Main-Belt Comets (MBCs) represent potential sources of water ice and other volatile materials, which can be converted into life support resources (explained as a use case later in the report for Oxygen production), propellants, and construction materials for future space missions.
- **Cost-Effectiveness:** The mission's focus on utilizing resources from MBCs aligns with the space industry's growing emphasis on cost-effectiveness and sustainability. By harvesting resources from nearby celestial bodies, such as MBCs, rather than transporting them from Earth, the mission aims to reduce the cost and logistical challenges associated with space exploration.
- **Technological Innovation:** The development and demonstration of space mining technology for extracting resources from MBCs represent a significant technological frontier in the space industry. Innovative approaches and advancements made during the mission have the potential to revolutionize future space exploration endeavors and pave the way for commercial space mining operations.
- **Scientific Exploration:** Beyond resource utilization, the Main-Belt Comet Mining Mission contributes to scientific exploration by providing valuable insights into the composition, origins, and evolution of comets. Studying MBCs can offer new perspectives on planetary formation processes and the distribution of water and organic materials in the solar system, furthering our understanding of the universe's history.
- **Commercial Opportunities:** The successful extraction and utilization of resources from MBCs open up new

commercial opportunities in space. Companies involved in space resource utilization, asteroid mining, and in-situ resource utilization (ISRU) stand to benefit from the knowledge and technology developed during the mission, potentially leading to the emergence of new space industries and markets.

II. MISSION STATEMENT & OBJECTIVES [SIBTAIN ALI]

To ideate the concept of mining and exploration of Main-Belt Comets (MBCs) in the asteroid belt, driven by a commitment to advancing scientific knowledge and unlocking the vast potential of space resources for further possibilities of space exploration. The mission aims to retrieve samples of volatile materials and mined resources from MBCs and safely transport them back to Earth, fostering insight into questions concerning the origin of Earth's water.

A. Primary Objective

To retrieve samples of volatile materials, such as water ice and organic compounds, and get insight into the origin of Earth's water.

B. Secondary Objectives

- 1) **Identifying and Locating More MBCs:** Initiate efforts to identify and locate additional Main-Belt Comets within our solar system.
- 2) **Demonstrate Space Mining Technology:** Conduct and determine the technical feasibility of mining and extracting valuable minerals contained in regolith, contributing towards future space mining missions.

C. Requirements

While the high-level mission requirements are mentioned in Table I, the subsystem level requirements are detailed later in the Appendix section XIII-A.

TABLE I
HIGH-LEVEL REQUIREMENTS

ID	HIGH LEVEL REQUIREMENTS
SYS-001	The system shall operate for 5 years
SYS-002	The system shall reach the asteroid belt and the targetted Main Belt Comet (MBC)
SYS-003	The system shall generate, store, and distribute power to all subsystems
SYS-004	The system shall maintain its temperature within its operational range
SYS-005	The system shall be compatible with the launch platform
SYS-006	The system shall identify and locate further MBCs
SYS-007	The system shall return the volatile and mined resources back to Earth
SYS-008	The mission shall contribute to the scientific understanding of origin of Earth's water
SYS-009	The system shall establish communication link with the ground.

D. Expected Deliverables from the Mission

- 1) **Volatile Material Samples Return:** Secure transportation of samples containing volatile materials, such as water ice and organic compounds, from Main-Belt Comets (MBCs) back to Earth for detailed analysis.
- 2) **Space Mining Technology Demonstration:** Demonstration of innovative space mining technology, including robotic extraction rovers and ore retriever rockets, tailored for resource extraction from MBCs.

- 3) **Scientific Analysis and Research Findings:** Analysis of retrieved samples and scientific data to advance understanding of MBC composition and origin, leading to scientific publications and further exploration efforts.
- 4) **Identification of Further Main Belt Comets:** Identification and exploration of additional main belt comets within the solar system, expanding scientific knowledge and potential targets for future exploration missions.
- 5) **Composition Analysis of Mined Regolith:** Detailed analysis of the composition of mined regolith from MBCs to assess its suitability for resource utilization in future space missions, contributing to the development of sustainable space exploration strategies.
- 6) **Ore-Retriever Development:** Designing and validation of a secure sample ore-retriever for transporting volatile materials from Main-Belt Comets (MBCs) back to Earth.
- 7) **Navigation System:** Validation of an advanced navigation system, enabling precise spacecraft maneuvering within the asteroid belt and approach to target MBCs for resource extraction.
- 8) **Reliable Communication Link:** Establishing a communication system to ensure continuous connectivity between the spacecraft and the ground station, facilitating seamless transmission of mission data, telemetry, and commands.

III. SIMULATION FRAMEWORK [ALESSANDRO TINUCCI]

A. GMATLAB

With the aim of capturing the complexity and the numerous interfaces present in complex systems, as well as speeding up the workflow for the preliminary design of our system, a new simulation framework was developed.

Having lots of interfaces means lots of dependencies, and that usually means an iterative process where the different parameters are calculated through a back and forth of simulations of the different subsystems compromising the complete spacecraft. This is usually a time intensive task that takes away from the design process and thus is an unwanted effect that is better minimized.

In the field of computational algorithms for the optimization of multivariate cost functions, Montecarlo simulations are probably one of the most common thanks to their simplicity. Generally, such algorithms can be broken down in the following steps:

- 1) Selection of inputs and outputs
- 2) Generation of representative cases
- 3) Simulation of cases
- 4) Evaluation of results

Where only steps 1. and 2. require human intervention, and steps 3. and 4. are a result of the physical modeling of the system through the numerical modeling of the different subsystems and the selection of representative cases to evaluate.

The basic structure of this framework and all of the subsystem modeling was done in MATLAB. For the orbital segment of the mission, GMAT was called through its API also from MATLAB.

In our particular case, the first step left us with a total of more than 40 parameters or degrees of freedom, with a given range of values for each, to be optimized for the system. This meant that if we were to simulate the full range of combinations, around 10^{14} cases would have to be simulated. This is obviously unfeasible even for modern computing machines, and therefore some educated simplifications had to be made. In our case only bi-linear relationships between every pair of parameters were simulated, that brought down the number of cases to a doable 10^6 .

This was done through the use of a so-called covariance matrix compromised of boolean values that describe if a relationship between any two given parameters exists (such as mass of propellant and engine selection) or not (communication system and ISP of the main engine). Further refinement of this matrix could be made to have a more complete and representative set of samples that better cover

the whole possible design state space.

A schematic overview of the complete simulation framework, GMATLAB, is given in Fig. 1:

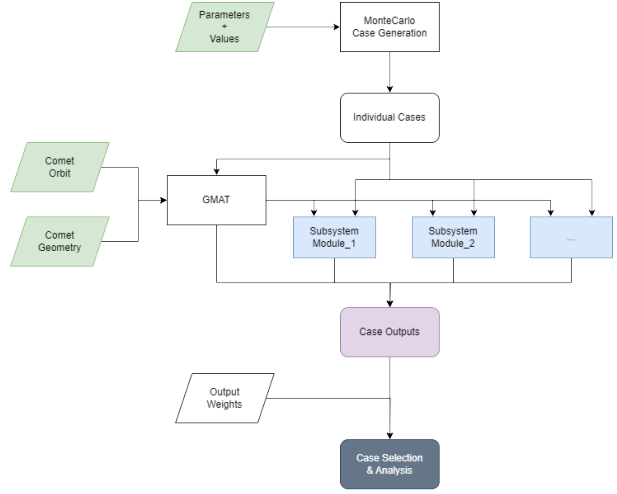


Fig. 1. GMATLAB Functional Diagram

Where in green are the inputs provided, in blue the different modeled subsystems and in purple and gray, the outputs and final best case respectively. The specifics of each subsystem model and the orbital segment are explained in more detail in the following sections.

Naturally, after each case is ran, a number of output values are saved in order to later assess their individual performance. To finally select a best case out of all of them a performance value is given to each case. This is calculated through a weighted sum of the normalized output values of each output.

The weights were user defined based on the desired optimization goals. Some obvious examples are minimizing the propellant mass required, minimizing the total power consumption needed or maximizing the ore to be retrieved.

All in all, this framework leverages the usefulness of Montecarlo simulations while still enabling a fast enough simulation rate through the use of powerful computing systems. The complete number of around 10^6 cases was simulated in just under 18 hours.

IV. MISSION ANALYSIS & DESIGN

A. Comet Selection [Leo Eitner]

An MBC is a body from the main asteroid belt that has been observed, on more than one occasion, to release a trail of dust when it passes through its periapsis. This indicates that the most probable cause for the dust trail is ice sublimation, meaning that the body is a comet. Additional observations in different parts of the light spectrum help eliminate cases where the dust trail is caused by rotational disintegration, thermal fracturing, or dehydration cracking.

Although many asteroids are under suspicion, currently there are only 10 confirmed MBCs. To proceed with the mission design, a specific MBC had to be chosen for exploration. Two main criteria were taken into account when doing this:

- **Size** - the greater the body, the stronger its gravity, making it easier to operate on its surface and to maintain a stable orbit around it.
- **Stability** - MBCs whose dust trail is suspected to be caused by more than just sublimation were ruled out due to surface instabilities. Additionally, bodies that are part of a binary asteroid system were also not considered due to complexity in orbit design and maintenance as well as surface instabilities from tidal forces.

In the end, MBC 324P/La Sagra (P/2010 R2) was chosen as the mission target [10].

B. Concept of Operations [Anibal Guerrero]

The spacecraft is separated into modules:

- **L**: Launcher - not part of the spacecraft but responsible for launching to GTO.
- **OM**: Observation Module - module with payload cameras, responsible for imagery and general observation strategies.
- **MM**: Main Module - contains the mining payload to be deployed to the comet. Responsible for transporting the regolith sample back.
- **ER**: Extraction Rover - mining payload responsible for regolith extraction.
- **OR**: Ore Retriever - regolith storage unit (where ER deposits regolith).

Comet Explorer's concept of operation is the following:

- 1) **Launch to GTO**: The Starship launcher takes the spacecraft to GTO, where the spacecraft will deploy and start the deployment sequence.
- 2) **Travelling to a Near-Comet Orbit**: The **OM** will transport the spacecraft to a near-comet orbit, at which point it will detach from the rest of the spacecraft, performing observation duties while the mission carries on in parallel.
- 3) **Near-Comet Orbit to Low Comet Orbit**: The **MM** now takes charge of the propulsive requirements, bringing the

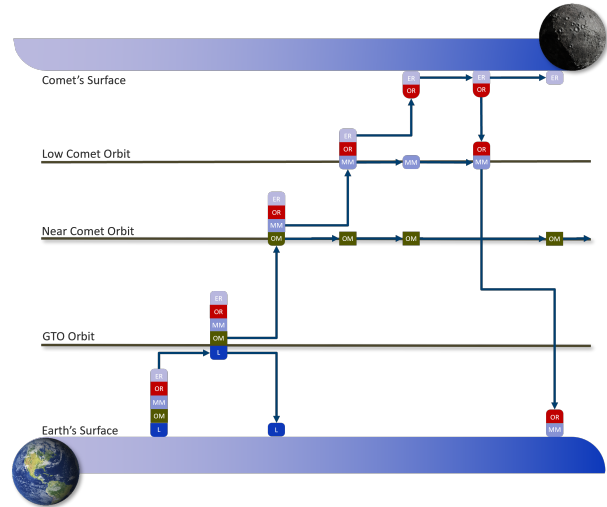


Fig. 2. *Comet Explorer's* Concept of Operations.

spacecraft to a low comet orbit close to *Comet 324P/La Sagra*. The objective is that the spacecraft orients itself into a position and orientation optimal for **ER** and **OR** deployment.

- 4) **Miner Modules Landing**: **ER** and **OR** land on the comet's surface. For the time required to obtain the desired regolith mass, mining will occur on the surface of the comet. After mining is completed, the **ER** and **OR** will assemble together and return to the **MM** that was in a maintenance orbit, waiting for these modules.
- 5) **Return to Earth**: **MM** takes the remaining spacecraft back to Earth, where sample can be processed and scientifically studied. This part of the concept of operations will only be present for the initial technology demonstrator, as long term goals of extraterrestrial mining is for space ISRU, without the requirement of returning to Earth.

C. Orbit Design [Alessandro Tinucci]

One of the key aspects of the mission profile considered is obviously that of the trajectory design to and from the comet. For that, three different phases were determined:

- 1) Launch and Initial Orbit (Earth)
- 2) Interplanetary Orbit (Earth - Comet)
- 3) Final Orbit (Comet)

Each section was calculated using a different approach that best suited the particular needs. Notably, the trajectory from the comet to Earth and posterior reentry were not considered separately and were instead considered inside the Interplanetary Orbit segment.

1) *Earth Orbit*: For the first section of the orbital trajectory and based on current available information on the possible capabilities of the Starship launch system, a Geostationary Transfer Orbit (GTO) of the following parameters was considered.

TABLE II
INITIAL ORBIT PARAMETERS

Perigee [km]	Apogee [km]	Inclination [$^{\circ}$]
6563	42157	27

This is of course completely dependent on the final performance offered by Starship and given the total take-off weight of the spacecraft, not trivial. Nonetheless, it was considered a fixed parameter in the consequent design choices.

Based on previous missions of similar profiles, this is a realistic representation of what could be expected from the launch system.

2) *Interplanetary Orbit*: The second and most complex orbit segment was that of the interplanetary transfer between earth and the comet. Given the size and weight constraints, minimizing the ΔV requirements and thus the propellant weight is a crucial aspect of the mission. And small differences in the trajectory design can greatly alter the feasibility of the project.

Proper studies of similar orbital profiles are time intensive and require a lengthy study of the wide range of possible trajectories available, while varying parameters such as the number of burns, their type, the time-frame considered and, most probably, also fuel-efficient maneuvers such as gravity assists.

Given our time constraints, this was not a possibility. And some simplifications had to be made.

GMAT was chosen as the simulation tool and a custom numerical algorithm was developed to study the launch window opportunities and elaborate a numerical *porkchop* plot, establishing the basis of the orbital analysis and providing some initial numbers for the propulsive needs and the required time-frame of the mission.

Unfortunately, the modification and addition of celestial bodies into the GMAT framework is not as straightforward as it could seem, and in order to accurately simulate the behavior of our desired comet, three different files had to be created to provide the software the required information. These were:

- PCK File (Provided as a plain-text .tpc file)
- SPK File (Provided as a plain-text .bsp file)

- FK File.

They are all used by the NAIF SPICE Toolkit that GMAT uses underneath for many orbit related calculations.

Out of these, the most important one and easier to obtain is the SPK file. It provides GMAT with the ephemeris of the comet and is readily available for download from NASA's Horizon Systems App (<https://ssd.jpl.nasa.gov/horizons/app.html/>).

The PCK file, a SPICE P-Kernel file, was then needed to provide information on the comet's orientation, size and shape. This was obtained through manual modification of a preexisting file, where assumptions for the values of our comet were added.

The orientation models express the direction of the pole and location of the prime meridian of a body as a function of time. The size/shape models represent all bodies as ellipsoids, using two equatorial radii and a polar radius. Spheroids and spheres are obtained when two or all three radii are equal.

Lastly, an FK File was required. This file, which stands for Frame Kernel, is the one responsible for providing the definition of the different reference frames used in the simulation. And it is used in particular by GMAT to calculate eclipses.

Creation of this file proved difficult. For some still unknown reasons GMAT refused to read the modified files, while providing little to no information on the reason it refused to do so, and after a lot of trial and error the effort was scraped. The amount of troubleshooting required for the little extra information that it provided was deemed not worth it.

And so, the comet modeling in GMAT was finalized with the PCK and SPK files, and the eclipse times were decoupled and calculated analytically afterwards.

The algorithm used was coded using GMAT's custom scripting language allowing fast automation of the setup process. It also employed the custom VF13AD Optimizer, a SQP-based Nonlinear Programming solver provided by Thinking Systems, Inc. instead of the usual Boundary Value Solver packaged with the software. This provided many advantages among which is a better convergence behavior even with a higher number of variables.

A multiple-shooting method that patched two spacecrafts, one propagating forward in time from Earth and the other propagating backwards in time from the comet was used.

As inputs of the method we considered: the initial state of the spacecraft (given just by its position), the departure date, the arrival date and the final state of the spacecraft, assumed

to be at a distance of 1000 km from the comet. Having both initial and final states fixed and both dates taking their values from a specified range we were interested in simulating in order to later elaborate the *porkchop* plot.

The logic loop followed can be schematized as:

- 1) Vary departure date and arrival date
- 2) Optimization loop

a) Vary:

- Initial v_x, v_y, v_z in relative frame between space-crafts
- Arrival v_x, v_y, v_z in relative frame between space-crafts

b) Propagate $t = (t_{arrival} - t_{departure})/2$

c) Constraint:

- ForwardSC v_x, v_y, v_z = BackwardSC v_x, v_y, v_z in relative frame between space-crafts
- ForwardSC p_x, p_y, p_z = BackwardSC p_x, p_y, p_z

d) Minimize Cost

3) Output: Initial v_x, v_y, v_z and Arrival v_x, v_y, v_z

4) Circularize: burn retrograde until $e = 0.9$

Where the cost to be minimized is the sum of the magnitudes of the departure and arrival velocities,

$$Cost = \sqrt{v_{1_i}^2 + v_{1_j}^2 + v_{1_k}^2} + \sqrt{v_{2_i}^2 + v_{2_j}^2 + v_{2_k}^2} \quad (1)$$

Storing the departure and arrival velocity vectors obtained by each pair of departure and arrival dates, a matrix can then be constructed that gives the wanted *porkchop* plot by summing the ΔV of the first impulse and the final circularization burn with:

$$\Delta V_{\text{interplanetary}} = \sqrt{(v_{\text{GTO}_i} - v_{\text{opt}_i})^2 + (v_{\text{GTO}_j} - v_{\text{opt}_j})^2 + (v_{\text{GTO}_k} - v_{\text{opt}_k})^2} \quad (2)$$

Where v_{opt} denotes the calculated departure velocities. Finally, with the code completely set up, a simulation was ran and results were obtained.

As can be easily observed, the usual porkchop shape that gives name to the famous plot is not present in the results obtained. Two are the factors that could be responsible for this: first, the purely numerical aspect of the algorithm used; and second, the fact that in order to speed up the simulation, a limit was set on the number of iterations the optimizer was allowed to take, making so that not all solutions were perfectly converged.

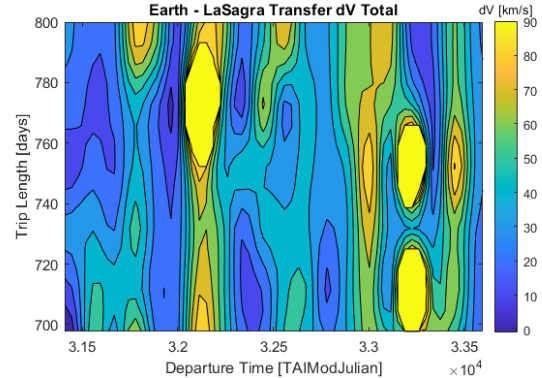


Fig. 3. Earth - LaSagra Numerical Porkchop Plot

The purely numerical aspect of the algorithm could cause that the solution would sometimes meant propagating through the earth after the initial burn. This was justified by the fact that given the time-frame of the mission, waiting for the spacecraft to orbit a fraction of the orbit up to a point where the calculated burn would not go through Earth didn't mean a substantial change to the overall profile.

With that in mind, a more precise and slightly modified run was done afterwards to validate further the final values. The main changes were allowing the optimizer to also modify the arrival date to its optimum instead of fixing it and choosing a finer time-step. A snapshot of the evolving cost value along with the final values obtained can be seen in the following figures.

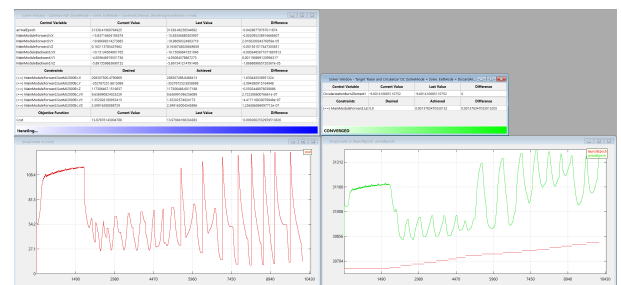


Fig. 4. Interplanetary orbit algorithm progress in GMAT.

Giving the final values that were used:

TABLE III
INTERPLANETARY BURN PARAMETERS

Parameter	Value	Units
Departure Date	Aug 2030	-
Trip Duration	600	days
Main Burn	~ 7	km/s
Circularization Burn	~ 2	km/s
Return Burn	~ 4	km/s

In a similar way but in reverse, going from the comet to earth, was the reentry calculated. No further insights were

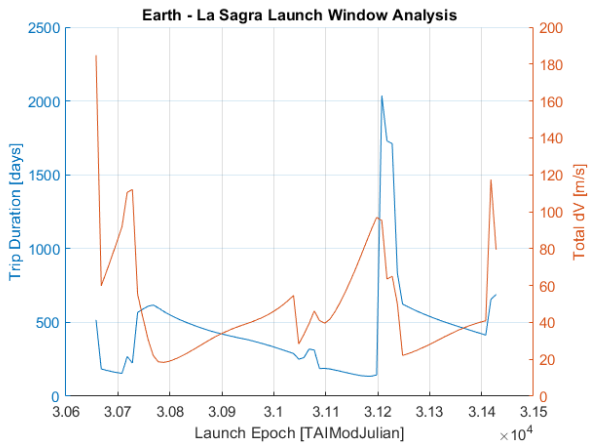


Fig. 5. Final transfer orbit analysis values.

gained with that approach and is the main reason why it was not considered separately.

Again, a consequent and more in-depth study using these values as a starting point is not only possible, but also recommended.

3) Comet Orbit:

Although simpler in the usual considerations that need to be taken into account, the low gravitational pull of the comet did pose some problems in the stability and feasibility of its orbit. Having only an estimated gravitational parameter μ of around 60, properly orbiting the body is not a realistic option. And again, carrying out a more in depth study of resonance points, possible halo orbits around stable points and similar considerations should be made.

For the time being some simplifications were needed and the simulation was carried out with a purely numerical approach. Its orbital parameters were iterated upon with the Montecarlo simulation of GMATLAB, taking into account its effects and interfaces with the rest of the subsystems (eclipse times, distance to comet, etc.). And from a set of a possible set of low altitude orbits, an standard orbit with the following parameters was used:

- SMA: 100 km
- i: 0°
- e: 0°

One of the main aspects for this selection was the proximity to the comet, that reduced the requirements on the many optical payload design considerations. Indeed, given the orbital model and the constraints that were introduced, there was no lower bound for the optimal height of the orbit. And a compromise, based also on past missions that have carried out similar orbits to comets, was arrived at.

D. Payload Strategy

1) *Observation [Leo Eitner]:* The Main Module will host several optical sensors to be able to obtain the information it requires to perform its mission.

- **ASTROhead Cam from JenaOptronik:** A camera that captures the light spectrum in the visual range. It will provide deep-space real-color pictures and, most importantly, monitor the development of the mission on the MBC's surface. This information will then be used to communicate with the Rover and the Ore Retriever and allow for some adaptation room during the mission. Additionally, it can also help with navigation if an extra star tracker is required.

This camera has been used in several missions already and offers two different FoVs that can be altered during flight. This allows for a more personalized camera configuration, depending on the environment it will be exposed to.

- **HAWAII 2RG from Teledyne:** A sensor for capturing the infrared range of the light spectrum, whose main objective is to evaluate the hydration levels of the surface regolith on the comet. It will record the spectrum mainly around the $3 \mu\text{m}$ range, which is the wavelength at which the water molecule reflects the most light.

This camera will be used to grade the surface of the comet and identify the areas with the most amount of ice. This information will then be fused with the LIDAR data and used to choose the landing spot, as well as to guide the rover to and on the mining grounds.

No COTS camera was available for this application. Therefore, it will have to be developed specifically for this mission. The diagram shown in Figure 6 was used to compute the required focal length (fl) and Equation 4 allows the calculation of the minimum required lens aperture (A) for this application [12]. The desired ground sampling distance (GSD) was chosen to be the rover's size ($\approx 1 \text{ m}$) to allow for precise instructions during operation. Table IV shows the outcome of the calculations.

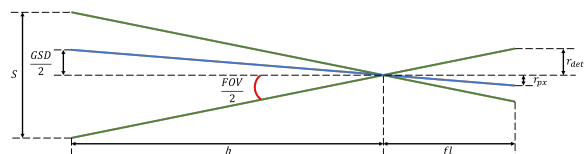


Fig. 6. Optical payload design diagram.

$$A = 2,44 \frac{\lambda}{GSD} \frac{h}{fl} \quad (4)$$

These values were obtained with a combination of 9 detectors linearly arranged, which together will work as a single multi-element whiskbroom sensor. The detector chosen is specially designed to be easily integrated into

TABLE IV
IR CAMERA SPECIFICATIONS

GSD [m]	Focal Length [m]	FOV [$^{\circ}$]	Lens Aperture [m]
1	1,8	10,5	0,4

a multi-sensor setup. To achieve the big required focal length a combination of mirrors will be used.

- **LEIA from MDA:** The LIDAR will be used to map the roughness of the comet's surface. This information will be used to grade the surface in terms of flatness, which will then be merged with the IR sensor data to find the optimal landing and mining areas on the comet's surface. Additionally, it will also be used for the rendezvous between the Ore Retriever and the Main Module after the mining has finished, providing the relative distance between the modules.

This sensor was specially designed for rendezvous and Moon landings, which can be adapted to our mission objectives. It is going to be integrated into ESA's LunaResurs Lander, and therefore be flight-proven before this mission.

2) Mining [Anibal Guerrero]:

In the pursuit of resource utilization beyond Earth, humanity stands at a pivotal juncture. An ever-growing demand for rare minerals and the necessity for sustainable practices is pushing humanity towards the exploration of celestial bodies. In this case, comets present an unparalleled opportunity. Comets are icy remnants from the early stages of our solar system, and harbor a wealth of resources crucial for scientific research and future space endeavors. However, accessing these resources in the demanding and chaotic environment of space poses formidable challenges.

Comets and asteroids entail low, irregular gravitational environments, abrasive dust particle cloud propagation, high exposure to radiation, and enormous differences in luminosity due to the rotational velocities of these Solar System Small Bodies (SSSBs). These environmental effects are a constraint to the strategy to follow in sample collection.

To address these challenges, the mission embarks in the footsteps of other pioneers, and harnesses the state-of-the-art developments in robotics and advanced mining technology. At the forefront of our payload strategy is the Regolith Advanced Surface Systems Operations Robot (*RASSOR*), a versatile and highly efficient mining robot specifically designed for extraterrestrial exploration in low gravitational environments. *RASSOR* represents the culmination of years of research and development, embodying the ingenuity and innovation essential for space exploration in the 21st century. [13], [14].

RASSOR Physical Properties

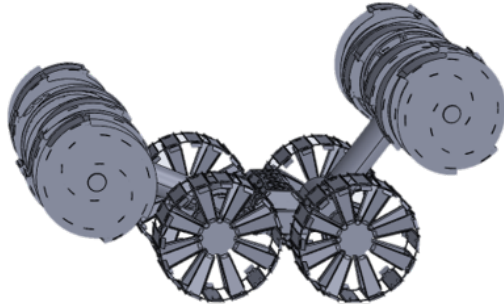


Fig. 7. RASSOR: Regolith Advanced Surface Systems Operations Robot

The RASSOR appears to be a suitable method for mining for several reasons:

- **Adaptability:** RASSOR is designed to operate in an extraterrestrial environment, specifically on the Moon. Its tank tread mobility system allows it to navigate and excavate in lunar regolith effectively.
- **Excavation Efficiency:** The dual counter-rotating bucket drum design of RASSOR minimizes excavation forces, allowing it to collect and transport regolith efficiently. This design helps in reducing the reaction forces on the robot, making it suitable for low-gravity environments.
- **Mining Depth Capability:** RASSOR is equipped to mine both the top 5 cm of surface regolith for nominal operations and up to 1 meter deep for icy regolith mining. This flexibility allows it to access different layers of the lunar surface.
- **Remote Operation:** RASSOR can be controlled remotely using a driver station software on a laptop, enabling operators to oversee and control mining operations from a safe distance.
- **Self-Righting Capability:** The ability of RASSOR to self-right itself using its dual arm configuration adds to its robustness, especially in challenging lunar terrain.
- **Mission Duration and Recharging:** With a five-year mission duration, RASSOR is designed to operate for an extended period. It uses rechargeable batteries that can be replenished at the lander between mining treks, ensuring sustained operations.
- **Cameras for Monitoring:** Equipped with one or more cameras, RASSOR provides visual monitoring of its operations, aiding in real-time decision-making and control.

3) Comet 324P Chemical Composition [Anibal Guerrero]:

Comets generally consist of a mixture of ices and other volatiles. Due to the limited resources in academic efforts towards research in comets, assumptions must be made. In this case, average chemical compositions must be assumed, to understand what can be sampled and to identify regions of interest. [3], [16].



Fig. 8. RASSOR excavating a slot trench in BP-1.

TABLE V
KEY TECHNICAL PARAMETERS OF RASSOR

Parameter	Value	Unit
Power Source	Li-ion Battery	-
Battery Capacity	1,410	Whr
Max Driving Slope	20	
Max Obstacle Height	75	cm
Regolith Delivered per Trip	90	kg
Max Speed	49	cm/s
Trips per Charge (100m)	20	Trips
Dry Mass	67	kg
Energy per Delivered Regolith	0.761	Whr/kg

According to the limit research and sampling of comets available, Table VI is derived, with the chemical composition that is to be expected for comet 324P/*La Sagra* [17], [7], [4].

Where the methods used are:

- R: Spectroscopy
- IR: Infrared Spectroscopy
- MS: Mass Spectrometry
- UV: Ultraviolet Spectroscopy
- V: Visible Spectroscopy

And the origin are:

- P: Proximal. Indicates that the measurement or observation is made from a proximal location, typically from or near the comet.
- D: Distal. Indicates that the measurement or observation is made from a distal location, often from a distance, such as Earth-based observations or telescopic measurements.

As it can be noted from Table VI, there is an abundance in ice in the comet. Knowing that the approximate weight percentage of H_2O is 80%, means that 80% of the total mass available in the comet is composed of H_2O molecules.

4) Example Use Case [Anibal Guerrero]:

An example use case of how resources from the comet could be utilised, is to provide oxygen to the ISS crew. In this example, it is calculated how much regolith should be extracted to convert the ice into sufficient oxygen for an assumed ISS crew of 6. This is the average crew year-round, for a year [28].

To extract the H_2O molecules from the ice, the regolith sample is to be collected. Due to the presence of other volatiles, the sample must be purified. In this case, the purification method followed were water is extracted is the *Pressure Swing Adsorption (PSA)* method. In *PSA*, the gas mixture is passed through an adsorbent material under high pressure. The adsorbent selectively retains certain gases while allowing H_2 and/or O_2 to pass through. The pressure is then reduced to release the purified gas. Some advantages of *PSA* are its simplicity, compactness, and no requirement of cryogenics. It is relatively simple and can operate in a cyclic manner, are originally designed to be compact and lightweight, and operates at ambient pressures, avoiding the need for cryogenic systems.

Then, the process of Proton Exchange Membrane (*PEM*) electrolysis can be employed. In *PEM electrolysis*, an electric current is passed through water (H_2O) in an electrolysis cell equipped with a proton exchange membrane. This membrane separates the two electrodes and allows only protons (H^+) to pass through while blocking the passage of gas and liquid. When the electric current is applied, water molecules near the anode undergo oxidation, releasing oxygen gas (O_2) and positively charged hydrogen ions (H^+). Meanwhile, at the cathode, hydrogen ions gain electrons and form hydrogen gas (H_2). The *PEM* separates the oxygen and hydrogen gases produced during electrolysis, allowing them to be collected separately.

Limitations of *PEM electrolysis* include its dependency on a reliable source of electricity, which may be challenging in remote locations such as comets. Additionally, high efficiency is required to ensure the economic feasibility of large-scale oxygen production using *PEM electrolysis*.

However, *PEM electrolysis* offers several advantages over other methods. It is a clean and environmentally friendly process, as it does not produce any greenhouse gases or other harmful emissions. It can also be operated at relatively low temperatures and pressures compared to other electrolysis methods, reducing energy requirements and equipment costs. Furthermore, the use of a proton exchange membrane allows for the selective separation of oxygen and hydrogen gases, resulting in high purity oxygen production.

Additionally, the extracted hydrogen as a byproduct, can be used for various purposes, including as a propellant for rockets, for metal reduction processes, or for power generation in fuel cells.

TABLE VI
COMPONENTS IN APPROXIMATE WEIGHT PERCENTAGE, METHOD OF ANALYSIS, ORIGIN, AND MIXING RATIO RANGE EXPECTED TO BE FOUND IN COMET 324P/LA SAGRA

Component	Approx. Weight %	Method	Origin	Mixing Ratio Range (M.R.%)
Water (H_2O)	80	R, IR, MS	P	100
OH	-	R, IR, UV	D	100
CO	Varies	R, IR, UV, MS	P, D	0.4 – 30
CO_2	Varies (0.01% to 20%)	IR, MS	P	2 – 6
CH_4 (Methane)	Varies	IR	P	0.14 – 1.4
C_2H_2	Varies	IR, MS	P	0.2 – 0.5
C_2H_6	Varies	IR, MS	P	0.11 – 0.67
CH_3OH (Methanol)	Varies	R, IR, MS	P	1 – 7
H_2CO	Varies	R, IR	P	0.2 – 0.6
NH_3 (Ammonia)	Varies	R, IR, MS	P	0.5 – 1.5
HCN	Varies	R, IR, MS	P	0.02 – 0.15
NH	Varies	V	D	0.11 – 1.6
S_2	-	UV	?	0.0012 – 0.005
SO_2	-	R	P	0.2
SO	-	R	D	0.2
H_2S (Hydrogen Sulfide)	Varies	R, MS	P	0.2 – 1

In summary, these are the steps that involve the extraction and purification of oxygen:

- 1) **Regolith Extraction:** Collect regolith samples from the comet surface, which contain ice and various volatiles.
- 2) **Pressure Swing Adsorption (PSA):** Purify the regolith samples using the PSA method.
 - Pass the regolith sample through an adsorbent material under high pressure.
 - Selectively retain certain gases while allowing H_2 and/or O_2 to pass through.
 - Reduce the pressure to release the purified gas, containing water vapor and other volatile compounds.
- 3) **Proton Exchange Membrane (PEM) Electrolysis:** Perform PEM electrolysis on the purified gas to extract oxygen.
 - Set up an electrolysis cell with a proton exchange membrane.
 - Pass an electric current through the purified gas in the electrolysis cell.
 - Allow water molecules to undergo electrolysis, separating into oxygen gas (O_2) and hydrogen gas (H_2).
 - Collect the oxygen gas produced at the anode side of the electrolysis cell.

5) Use Case Calculations [Anibal Guerrero]:

All processes previously mentioned are not perfect. Therefore, efficiencies have to be taken into account. Table VII describes the practical efficiencies encountered from practical results in real mining processes.

TABLE VII
EFFICIENCIES OF ALL PROCESSES INVOLVED

Parameter	Value
Recovery rate of the PSA process	60%
Oxygen purity	98%
Weight content of water within comet 324P/La Sagra sample	80%
PEM Electrolysis efficiency	80%

Using the data compiled in Table V and Table VII, the mass requirements of the regolith at each step of the involved process for the specific use case, can be calculated and are found in Table VIII and Table IX for the regolith mass and RASSOR mission plan, respectively.

TABLE VIII
CALCULATIONS OF MASSES AND TRIPS REQUIRED FOR THEORETICAL USE CASE

Parameter	Value	Unit
O_2 Consumption per person per day	0.84	kg/pax/days
Total ISS O_2 Consumption	1,840.86	kg
H_2O Required for Electrolysis	4,141.96	kg
H_2O to be Purified through PSA	5,177.45	kg
Total Regolith to be passed through PSA	8,805.20	kg
Total Regolith Mass required	11,006.49	kg
Total Time for 1 trip	3.7	hours
# Trips required	138	-
Total Time Sampling	21.25	days

E. Payload Use Case - Surface Flatness [Alessandro Tinucci]

As a recreational exercise a simulation of what a practical use of the onboard payload system proposed for the mission could look like was carried out. The idea was that of using the information gathered by the LiDAR and optical cameras

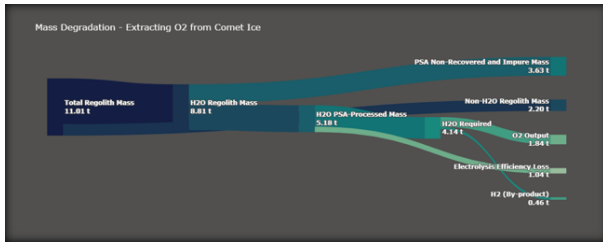


Fig. 9. Mass Degradation through O_2 extraction process from original regolith collected by RASSOR.

TABLE IX
RASSOR REQUIREMENTS AND MISSION INFORMATION

PARAMETER	VALUE	UNIT
Total Power Consumption	8,375.94	Whr
# of Batteries	6	-
Total Distance Travelled	27.6	km
Total Time Sampling	21.25	days
Current TRL	4	-
Expected TRL by 2029	6	-

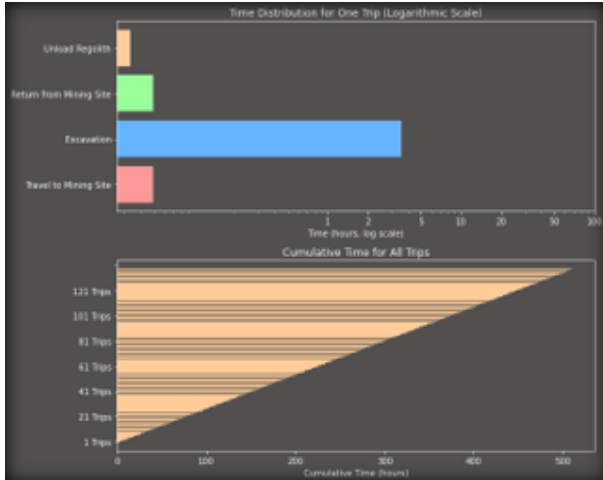


Fig. 10. Individual time required per RASSOR activity, and overall mining time.

to study the geometry and composition of the comet and evaluate possible landing configurations.

You can see in Fig.11 a 3d view of what would be gathered by the payload cameras. In this practical case, this are the x, y and z coordinates of a point cloud mapped in a 3d space. They were read from a Polygon File (.ply extension) of a sample comet. This extension was used primarily because of its extended use with 3d scanners and it's resemblance with the functionality of a LiDAR camera.

The cloud of points is then processed, gradients of the elevation and of the first derivative of the elevation are calculated through a weighted average of the dot product of the normal at a given point with the vector pointing to the nearby points. So that, in case that those nearby points fall

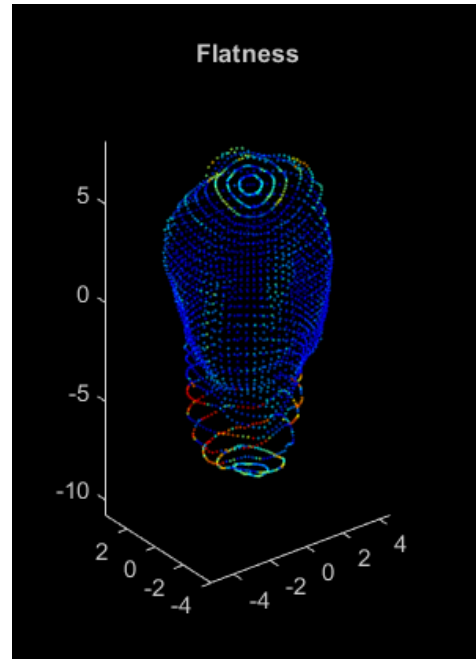


Fig. 11. 3D Scanned view of a sample comet.

in the normal plane, the dot product of the normal and the vector to the neighbor becomes zero and contrary if there is a big gradient. This is done for all points in a short amount of time, and the values for flatness stored in a different matrix. A similar processing could be done with the material composition of the comet. Those values of flatness are what give color to Fig.11.

The next step in the processing is that of translating this 3D information into a 2D projection for ease of use. In this case we chose Mercator projection because of familiarity, but analogous steps could be followed for any other type of projection.

After this is done again automatically the biggest area of lowest slope is automatically chosen, simulating what could be the OBCS's landing spot selection algorithm. The polygon that encircles the area is created and saved as a Shape File (.sph).

Finally, as a last step, we also incorporated this processing into the Montecarlo simulation carried out by GMATLAB, where the processed shape file was imported and the final comet orbit evaluated based on the percentage of this area that it covered, and the amount of time it spent over it with respect to the total orbit period. This simulates what could be an autonomous selection process that the spacecraft could carry out to determine its final orbit around the comet as it comes closer to it and the cameras are able to gather the information. Again, this could be used not just for landing zone analysis but also for resources localization with the proper data supplied.

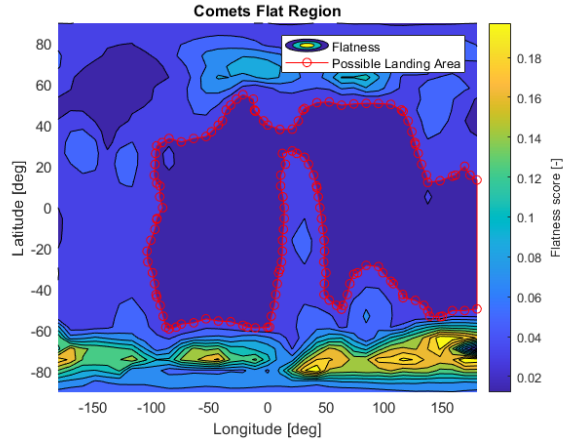


Fig. 12. 2D Analysis of landing zone.

An example of the implementation of this information into GMATLAB can be seen in Fig.13, where the percentage of area covered inside of the landing zone region selected is shown. Two horizontal stripes of higher coverage are seen on top and at the bottom because of the particular orbit that was chosen in this case, with an inclination of almost 30°.

As a last note, it can also be seen the higher concentration for the lower band at around 0° of latitude and at around -100° for the top one. This is due to the low number of orbits around the comet that were taken as a sample size. In this case just 3.

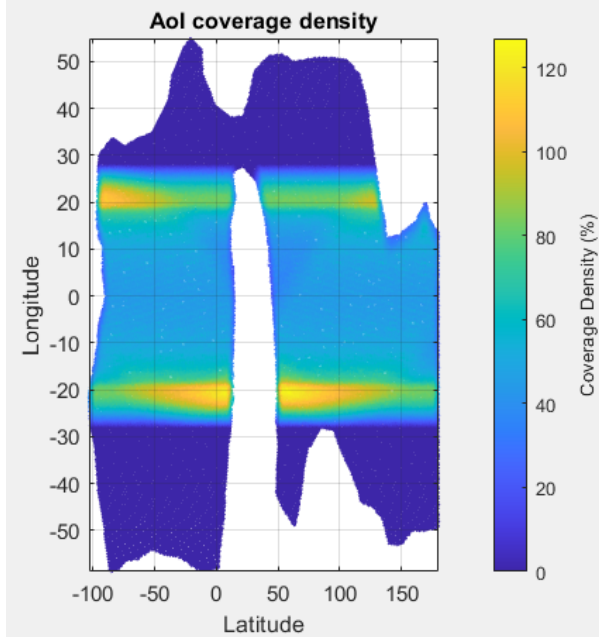


Fig. 13. Orbit analysis through area coverage.

V. SPACECRAFT SYSTEM DESIGN

A. Communication System [Leo Eitner]

The communication system is used to communicate with Earth as well as between modules. Within this system, there are two main data groups: the TT&C (telemetry, tracking, and command) and the science data. Both are equally important and deserve to be looked at individually.

1) Science data:

Science data is all the data collected by the payload during the mission from measurements and observations. This information is not essential to the mission itself. It is only transmitted by the spacecraft to Earth (downlink) and usually requires the highest data rates in the communication system.

For this link, the Ka-band was chosen because it is the highest frequency band used for satellite communication, allowing for the greatest bit rate, which is attractive for science data links. The more data one can transmit the more valuable the mission becomes. However, this band has some drawbacks, such as its high susceptibility to atmospheric conditions and, since it uses high frequencies, it also requires high transmitting power and/or high gain antennas to maintain error-free communication. The exact frequency selected was $f = 31,8$ GHz as this is within the allowed range from ITU [2], and is the frequency used by the selected ground stations network, DSN [25].

Regarding the COTS hardware, the following components were selected:

- **HRT150 by General Dynamics:** it was the only Ka-band transmitter found on the market.
- **Beamsat Horn Antenna by Picosats:** highest-gain Ka-band antenna found on the market.

These components themselves are not enough for a reliable link in the Ka-band at the range of distances that the communication is going to happen. Additionally, a horn antenna is highly directional and would require very high precision from both sides of the link for communication to be possible. A reflector is then required to increase both the gain and the aperture of the antenna.

The design driver of this link was the maximum achievable bit rate. Therefore, the maximum size reflector was chosen, as this gives the highest reflector gain. Since the Starship limits the size of its payload to a radius of 8 meters, this was chosen as the aperture of the reflector D . Additionally, a desired link margin of 20 dB was set as a requirement as it is normally done for links above 10 GHz [12].

The coding and modulation were selected from the available options from the used transmitter. Here, the combination of QPSK modulation and R-1/2 Viterbi coding was chosen as it leads to the highest link margin [12]. The final link margin, M , can be seen in Table X, calculated according to Equation 5, where a safety factor of $SF = 2$ dB was used to account for unmodelled losses.

The gain achieved by the reflector, G_{ref} , was computed using Equation 6, and the maximum bit rate, B_r , was calculated using Equation 7.

TABLE X
KA-BAND LINK BUDGET AND ACHIEVED BIT RATE.

E_b/N_0	Modulation/Coding	$(E_b/N_0)_{req}$	Margin	B_r
26,4 dB	QPSK/R-1/2 Viterbi	4,4 dB [12]	20 dB	1,2 kbps

$$M = \frac{E_b}{N_0} - \left(\frac{E_b}{N_0} \right)_{req} - SF \quad (5)$$

$$G_{ref} = 20 \log_{10}(D) + 17.8 + 20 \log_{10}(f[\text{GHz}]) \quad (6)$$

$$B_r = 10^{\frac{P_t - \frac{E_b}{N_0} + L_t + G_t + L_s + L_r + G_r - 10 \log(k) - 10 \log(T_s)}{10}} \quad (7)$$

where P_t , L_t and $G_t = G_{ref} + G_{antenna}$ are the power, losses, and gain of the transmitting system, L_r and G_r are the losses and gain of the receiving system, L_s is the free space loss given by $L_s[\text{dB}] = 147,55 - 20 \log(h) - 20 \log(f)$, k is the Boltzmann constant and T_s is the noise temperature of the receiving system.

2) TT&C:

This part of the communication system aims to transmit information about the health and status of each subsystem, as well as the position and orientation of the spacecraft. It is also used for remote control if required.

The chosen frequency band was the X-band as it is the highest frequency band that is immune to atmospheric effects, allowing for atmosphere-independent communication. This is especially important for TT&C as it is mission-critical information. The exact frequencies selected are $f = 7,145$ GHz for uplink and $f = 8,4$ GHz for downlink. Again these were chosen based on allowed ranges [2] and DSN availability [25].

Four links are established during mission operation:

- Earth - Main Module (Uplink)
- Main Module - Earth (Downlink)

- Main Module - Ore Retriever (Downlink)
- Ore Retriever - Main Module (Uplink)

For these links, all the components are COTS:

- **SDST by General Dynamics:** a TRL9 transponder used for communicating with Earth, both uplink and downlink. It requires low power but has a high enough transmitting bit rate for the low requirements for TT&C.
- **XLINK-X by IQ Spacecom:** a TRL9 transceiver that will be integrated both in the Main Module and the Ore Retriever, designed for CubeSats but easily adaptable for the links between the two modules.
- **X Band Antenna by IQ Spacecom:** a TRL9 4-patch antenna capable of receiving and transmitting at the same time. Again one is used in each module for the links between them.
- **Beamsat Horn Antenna by Picosats:** the same horn antenna used for the Ka-band link will be used to transmit and receive in the X-band.

The modulation and coding used were again selected from the available options on the chosen hardware. In the end, the same combination was used for every link, namely a BPSK modulation with RS Viterbi Coding, as this led to the highest link margin [12].

Equations 5, 6, and 7 were again used to compute the link budgets. Equation 8 was additionally used to adapt the gain of the horn antenna for the Ka-band to X-band frequencies, G . The resulting link budgets can be seen in Table XI.

$$G = 20 \log_{10} \left(\frac{f_{Ka}[\text{GHz}] \times 10^{\frac{G_{Ka}+2,8}{20}}}{f[\text{GHz}]} \right) - 2,8; \quad (8)$$

TABLE XI
X-BAND LINK BUDGETS.

Link	E_b/N_0 [dB]	$(E_b/N_0)_{req}$ [dB]	Margin [dB]
Earth - MM	100,0	2,7 [12]	95,3
MM - Earth	70,7	2,7 [12]	66,0
OR - MM	26,0	2,7 [12]	21,3
MM - OR	27,6	2,7 [12]	22,9

B. ADCS [Sibtain Ali]

1) *Attitude Dynamics:* The attitude dynamics of the satellite, which is considered as a rigid body, are computed using Euler's equation as [15]:

$$\underline{\underline{I}\omega} = \underline{\underline{I}\omega} \times \underline{\omega} + \underline{\underline{M}_d} + \underline{\underline{M}_c} \quad (9)$$

where $\underline{\omega}$ is the angular velocity, $\underline{\underline{M}_d}$ is the disturbing torque, $\underline{\underline{M}_c}$ is the control torque and I is the inertia matrix of the satellite defined as:

$$I = \begin{bmatrix} 155750 & 0 & 0 \\ 0 & 155750 & 0 \\ 0 & 0 & 87500 \end{bmatrix} \text{kgm}^2 \quad (10)$$

The numerical integration of this equation is then used to compute the spacecraft kinematics using Euler angles ϕ , θ , and ψ as the attitude parameters to obtain the attitude matrix. In particular, for this study the set $\mathbf{A}_{313}(\phi, \theta, \psi)$ is chosen which considers two rotations around the z axis and the middle one around the x axis of the inertial reference frame. The Euler angles from this set can be computed by integrating:

$$\begin{cases} \dot{\phi} = \frac{(\omega_x \sin \psi + \omega_y \cos \psi)}{\sin \theta} \\ \dot{\theta} = \omega_x \cos \psi - \omega_y \sin \psi \\ \dot{\psi} = \omega_z - (\omega_x \sin \psi + \omega_y \cos \psi) \frac{\cos \theta}{\sin \theta} \end{cases} \quad (11)$$

while, the $\mathbf{A}_{313}(\phi, \theta, \psi)$ can be computed as:

$$\mathbf{A}_{313} = \begin{bmatrix} c\psi c\phi - s\psi s\phi c\theta & c\psi s\phi + s\psi c\phi c\theta & s\psi s\theta \\ -s\psi c\phi - c\psi s\phi c\theta & -s\psi s\phi + c\psi c\phi c\theta & c\psi s\theta \\ s\phi s\theta & -c\phi s\theta & c\theta \end{bmatrix}$$

Using the Euler angles as attitude parameters it is important to consider the singularities that this decision brings. In fact, in this case, when $\theta = k\pi$ the inverse of the rotation matrix is not defined. Therefore, along with the computation of the \mathbf{A}_{313} matrix, also the $\mathbf{A}_{312}(\phi, \theta, \psi)$ is computed, so that, when the θ angle of the 313 set comes close to $k\pi$, the \mathbf{A}_{312} is used instead of the \mathbf{A}_{313} . This can be performed because the singularities for \mathbf{A}_{312} happen when $\theta = (2k+1)\frac{\pi}{2}$. The Euler angles of the 312 set can be obtained by integrating:

$$\begin{cases} \dot{\phi} = \frac{(\omega_y \cos \psi - \omega_z \sin \psi)}{\cos \theta} \\ \dot{\theta} = \omega_x \cos \psi + \omega_z \sin \psi \\ \dot{\psi} = \omega_y - (\omega_z \cos \psi - \omega_x \sin \psi) \frac{\sin \theta}{\cos \theta} \end{cases} \quad (12)$$

while the $\mathbf{A}_{312}(\phi, \theta, \psi)$ can be computed as:

$$\mathbf{A}_{312} = \begin{bmatrix} c\psi c\phi - s\psi s\phi s\theta & c\psi s\phi + s\psi c\phi s\theta & -s\psi c\theta \\ -s\phi c\theta & -c\phi c\theta & s\theta \\ s\psi c\phi + c\psi s\phi s\theta & s\psi s\phi - c\psi c\phi s\theta & c\psi c\theta \end{bmatrix}$$

2) Sensors:

The combination of sensors has been carefully selected out of those available, based on the accuracy requirements of the mission, see appendix XIII-A. This is one of the reasons why both the sun sensors and the star trackers have been chosen to overcome their drawbacks, as well as offer a combined high level pointing accuracy, especially during the launch and rendezvous of the ore retriever. As shown in Table XII, while the star trackers offer a much higher degree of accuracy, they are not very effective under direct sunlight, which is when the attitude determination is primarily dependent on the sun sensors. The choice of the gyroscope has been dictated by the gyro angular random walk, which is the measure of accuracy

and lower noise characteristics, as well as the fact that it offers 4-axes tetrahedral redundancy. The overall combination of sensors offers multiple redundancies so as not to hinder the success of the mission if any of them goes faulty.

TABLE XII
SENSORS AND THEIR STANDOUT PERFORMANCE PARAMETERS

Sensors	Parameters	Values
Gyroscope [23] - (1x4)	ARW	0.0002°/hr
	Range	±35°
	Power	40 W
	Mass	8 kg
Sun Sensor [21] - (5)	Accuracy	<0.02°
	FOV	128°
	Power	1 W
	Mass	0.33 kg
Star Tracker [18] - (3x2)	Accuracy	<0.001°
	FOV	20°
	Power	8.9 W
	Mass	3.55 kg

3) Actuators:

TABLE XIII
ACTUATORS AND THEIR STANDOUT PERFORMANCE PARAMETERS

Actuators	Parameters	Values
Thrusters (12)	Max Thrust	22 N
	Fuel Oxidizer	Hydrazine Nitrous Oxide
CMG [19] - (1x4)	Torque	60 Nm
	Momentum	30-45 Nms
	Power	30 W
	Mass	38 kg

The choice of actuators in Table XIII is carefully based on the magnitude of actuation required, as determined from simulation results in the later section V-B4, which are primarily dependent on the inertia matrix 10 of the satellite and initial tumbling velocity 14. For the satellite in consideration, it can be fairly easily deduced that momentum exchange devices are very much incompetent given their actuation limit, and therefore a very frequent need to be desaturated by thrusters. Hence, thrusters are chosen as primary actuators for major attitude correction, leaving the final precision to CMGs, which are in accordance with the simulation results, and have enough capacity to maintain pointing accuracy.

Assumption

One major assumption is that while thrusters are limited in their increment of thrust by the parameter 'minimum impulse bit', as well as are restricted by the minimum thrust they can provide. For the sake of simplicity in simulation, the thrusters are assumed to have the full range of thrust availability from 0 to maximum without relying on CMGs for precision, as in reality, and therefore giving an estimate of the propulsion effort required because the CMGs will eventually need to be desaturated for the equivalent amount of torque applied as shown in the simulation results.

Choice of Thruster

For the choice of the thruster, it was chosen to be bi-propellant, the same as the main propulsion system to share the mutual fuel reservoirs and avoid the dead weight of carrying extra structural mass. Moreover, they offer the extra margin of thrust availability for unforeseen attitude corrections and disturbance torques that may be experienced by the satellite in the asteroid belt. They are also preferred over other types for the following reasons:

- **Electrical Thrusters** are extremely power consuming, more or less 90% is devoted simply to keep it ready to use and only 10% is due to the thrust produced, therefore electric propulsion units are often coupled with extremely large solar panels.
- **Cold-Gas Thrusters** use a non-reactive gas, stored at high pressure (around 30 MPa), commonly use Nitrogen SP 70s or Helium SP 175s. Helium saves mass but is more prone to leakage and more expensive, not to mention the extra structural mass of tanks.

The configuration used is typical for a thruster attitude system, and involves 12 units arranged in the lower part of the satellite as shown in Figure 14 so that the rotations around the three axes are controlled by 4 thrusters each, thus offering redundancy.

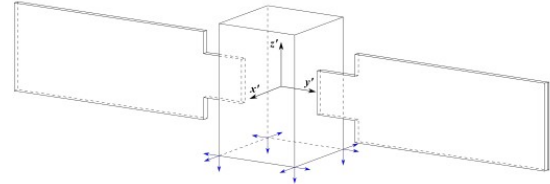


Fig. 14. Arbitrary satellite showing thruster configuration

The torque generated by the actuators can be computed as:

$$\underline{M}_{c_{\text{real}}} = [\hat{\mathbf{R}}] \underline{u}_{c_{\text{real}}}$$

where $[\hat{\mathbf{R}}]$ is the thruster configuration matrix which maps the torque action of each thruster and is computed as shown in Equation 13, while $\underline{u}_{c_{\text{real}}}$ is a vector that expresses the thrust allocated for each thruster.

$$[\hat{\mathbf{R}}] = \left\{ \begin{array}{ccc} r_1 \times f_1 & \cdots & r_{12} \times \hat{f}_{12} \end{array} \right\} \quad (13)$$

In order to obtain $\underline{u}_{c_{\text{real}}}$, first of all the ideal control torque needs to be computed using a simple "bang-bang" type controller [15]:

$$\underline{M}_{c_{\text{ideal}}} = -T \operatorname{sgn}(\underline{S})$$

where \underline{S} depends on each mission phase. Note that this controller type is similar to one used for fixed thrust jets, with the only exception that T corresponds to an ideal torque proportional to \underline{S} . In addition, the computation of \underline{T} follows a Schmitt-Trigger logic. Next, due to the fact that in general

the Moore-Penrose pseudo inverse cannot be used to solve $-[\hat{\mathbf{R}}]_c = \underline{M}_{c_{\text{ideal}}}$ because of the additional constraint of $\underline{u}_c \geq 0$, it is possible to use a general pseudo inverse defined as:

$$\underline{u}_c = -[\hat{\mathbf{R}}]^+ \underline{M}_{c_{\text{ideal}}} + \gamma \underline{w}$$

where \underline{w} is the null space vector of $[\hat{\mathbf{R}}]$, and γ is a scalar defined as:

$$\gamma = \max_{i=1,\dots,N} ([\hat{\mathbf{R}}]^+ \underline{M}_{c_{\text{ideal}}}) / w_i.$$

The last step is to check if the thrust allocated for each thruster expressed by \underline{u}_c is constrained between the minimum and maximum thrust admissible by each actuator and then build the final vector $\underline{u}_{c_{\text{real}}}$.

4) Control Algorithms and Simulation:

A block scheme of the simulation is shown in Figure 15, while the Simulink architecture can be seen in the appendix XIII-B.

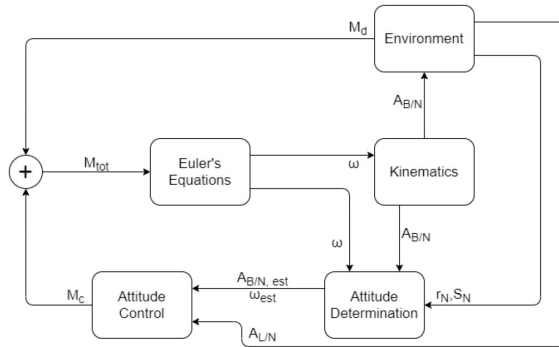


Fig. 15. Simulation Scheme

Detumbling - GTO

The initial tumbling velocity of the satellite right after launch, as shown in equation 14 is taken from the reference of the Rosetta mission [24]. Comparing the difference between the masses of the spacecraft in consideration and that of Rosetta, the referenced tumbling velocity is assumed to be an overestimate of the initial conditions considering the conservation of angular momentum, and therefore tests the actuators for overarching requirements.

$$\underline{\omega}_o = \begin{bmatrix} 0.8 \\ -0.6 \\ 0.5 \end{bmatrix} \text{ deg/s} \quad (14)$$

During the detumbling phase, the ADCS system must reduce the spacecraft's angular velocity almost to zero from the initial conditions. This is performed using the procedure described in Section V-B3. In particular, the ideal control torque expression used for detumbling involves the parameter $S = \omega$, therefore:

$$M_{\text{ideal}} = -\underline{T} \operatorname{sgn}(\omega) \quad (15)$$

The parameter \underline{T} is the ideal momentum couple in the three axis, and is obtained as:

$$\underline{T} = \underline{F} \underline{l} \quad (16)$$

where \underline{l} is the vector of the distance between the two forces, and it is expressed as:

$$\underline{l} = \begin{cases} 2 \cdot 4m \\ 2 \cdot 2.5m \\ 2 \cdot 2.5m \end{cases} \quad (17)$$

while \underline{F} is a function of the parameter \underline{S} , which in this case is equal to $\underline{\omega}$, indicates the amount of thrust that the thrusters need to provide to the system to detumble the satellite, and it is obtained using a Schmitt-Trigger-like logic, where i=x, y, z.

$$F_i = \begin{cases} F_{\max} & \text{if } |S_i| > S_{\max} \\ \frac{F_{\max} - F_{\min}}{S_{\max} - S_{\min}} (S_i - S_{\min}) + F_{\min} & \text{if } S_{\min} < |S_i| < S_{\max} \\ 0 & \text{if } |S_i| < S_{\min} \end{cases}$$

F_{\max} and F_{\min} are respectively the maximum and minimum thrust available from the each thruster, while S_{\max} and S_{\min} are arbitrary selected values that define the range of angular velocities in which the thrusters should be active. While in this case $S_{\min} = 0$ for the simplicity in simulation only relying on thrusters, in reality, it can be set to a value below which the CMGs should take command to completely detumble the satellite. While $S_{\max} = 1$ is considered as an extreme case that should require the maximum actuation, primarily because the mass of propellant carried by spacecraft as shown in section V-D4 can have extremely detrimental effects on the stability due to sloshing.

The thrust output between the two extremes of angular velocity is dictated by the concept of first-order sliding mode control, which is based on the ratio of thrust range to angular velocity and the corresponding actuation required at each time step to ensure a smooth decrease in tumbling velocity. It is worthy to note that while it is far from reality, it provides a decent insight into the capability of the ADCS system.

The results shown in Figure 16-19 show how the satellite is detumbled in about 3 minutes referencing the operational report of Rosetta Mission [24] and the corresponding change in Euler angles following the thrust output.

Pointing - GTO

The objective of the satellite attitude control system is to orient the spacecraft from the initial conditions toward Earth/Comet respectively. In particular, the x-axis of the body frame is required to be aligned with the x-axis of the Local Vertical Local Horizontal frame (LVLH). Therefore as the main performance parameter, the pointing error between them is chosen as:

$$\epsilon_{\text{pointing}} = \arccos [(\mathbf{A}_{B/N} \mathbf{A}_{L/N}^T \underline{x}_L) \cdot \underline{x}_B] \quad (18)$$

Where,

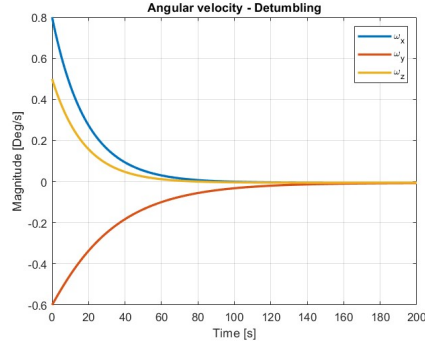


Fig. 16. Angular velocity variation

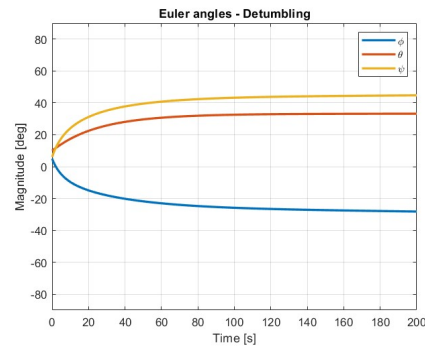


Fig. 17. Euler Angles variation

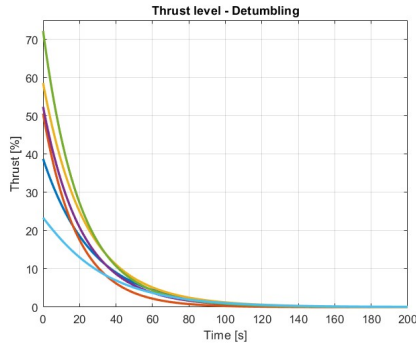


Fig. 18. Thrust Output

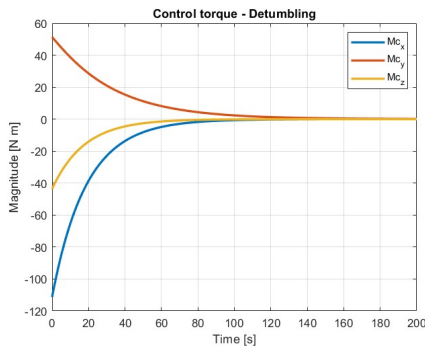


Fig. 19. Control Torque variation

$$\mathbf{A}_{B/N} = \text{body frame relative to inertial frame}$$

$$\mathbf{A}_{L/N} = \text{LVLH coordinate frame relative to inertial frame}$$

In addition, the angular velocity during the pointing phase must be the same as the LVLH frame, and is dependent on the period (T) of the orbit as:

$$n = \frac{2 * \pi}{T} (\text{rad/s}) \quad (19)$$

Therefore the desired angular velocity (for a use case of pointing x-axis to nadir point with continuous changing ω_z) and attitude matrix are:

$$\underline{\omega}_d = \{0, 0, n\}^T \quad \mathbf{A}_d = \mathbf{A}_{L/N} \quad (20)$$

The same procedure explained in Section V-B3 is used, however in this case the parameter S is the tracking control obtained using Lyapunov control function [15]:

$$\underline{S} = - \left[-k_1 \underline{\omega}_e - k_2 (\mathbf{A}_e^T - \mathbf{A}_e)^V + \underline{\omega} \times \mathbf{I} \underline{\omega} \right. \\ \left. + \mathbf{I} (\mathbf{A}_e \dot{\underline{\omega}}_d - [\underline{\omega}_e]^\wedge \mathbf{A}_e \underline{\omega}_d) \right] \quad (21)$$

with $\underline{\omega}_e = \underline{\omega} - \mathbf{A}_e \underline{\omega}_d$, $\mathbf{A}_e = \mathbf{A}_{B/N} \mathbf{A}_e$ and $(\mathbf{A}_e^T - \mathbf{A}_e)^V = \{A_{e2,3} - A_{e3,2}, A_{e3,1} - A_{e1,3}, A_{e1,2} - A_{e2,1},\}^T$.

The values of the tuning parameters k_1 and k_2 used for the pointing phase has been iteratively determined through simulation results as:

$$k_1 = 6, k_2 = 2$$

In order to obtain the value of T , the same Schmitt-Trigger-like logic procedure explained earlier in this section is performed, however, the values of $S_{\max} = 1$ and $S_{\min} = 3 \cdot 10^{-10}$ have been used. The following Figures 20 - 24 show how the pointing error is reduced and the corresponding changes in angular velocity. The continuous change in yaw angle ψ in Figure 21 shows the variation due to following the nadir point.

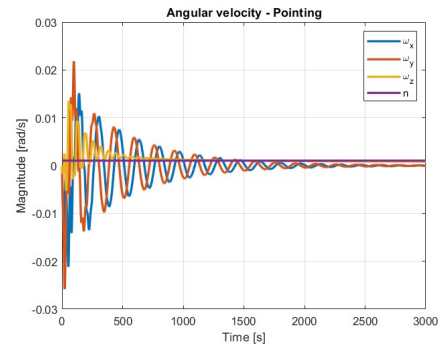


Fig. 20. Angular velocity variation

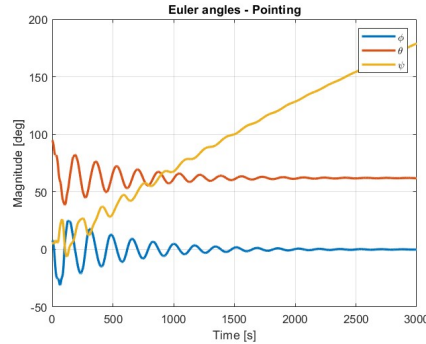


Fig. 21. Euler Angles variation

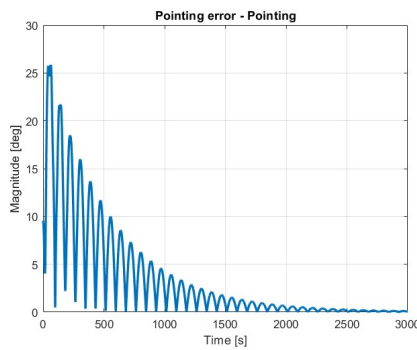


Fig. 22. Pointing Error

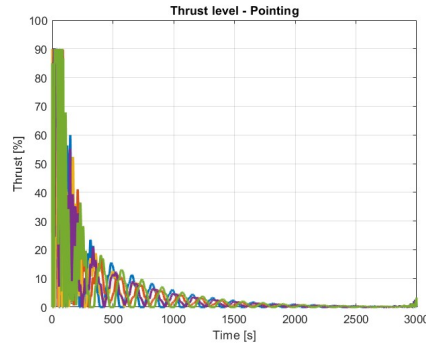


Fig. 23. Thrust Output

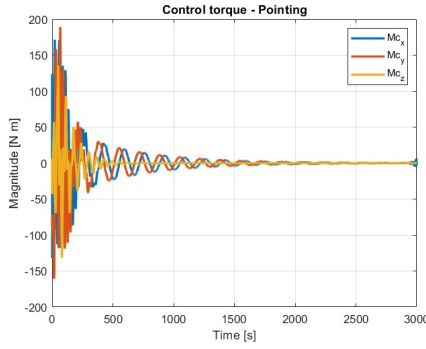


Fig. 24. Control Torque

Pointing - Comet

This section makes use of the same approach as in the previous section for the pointing phase in the GTO around Earth, except for making use of the orbit parameters around the comet as specified in section IV-C3, keeping the overall approach unchanged. These simulation results in Figures 25 - 26 offer greater insight into the performance reliability of the ADCS subsystem during the mining phase (21.25 days) around the comet, giving a reasonable estimate of the propellants required for a combined $\Delta V = 0.5$ km/s as mentioned in section V-E and catered for in the total mass budget in section V-D4.

The estimated disturbance torques in the asteroid belt are taken from [9] and added to the appendix in Figure 45. As can be seen, these disturbance torques are negligible in magnitude and can be used as a first approximation, therefore not requiring specific measures, even for increased orders of magnitude.

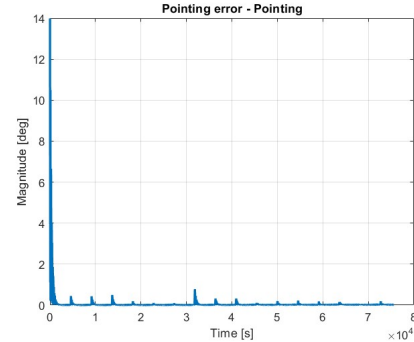


Fig. 25. Pointing Error

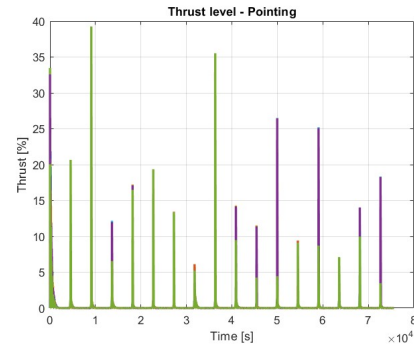


Fig. 26. Thrust Output (Impulses)

C. On-Board Computers & Software [Sibtain Ali]

The On-Board Computing System (OBCS) selected for the mission is shown in Figure 27 with the specifications detailed in Table XIV. This particular subsystem embodies hardware components meticulously tailored to the needs

of extraterrestrial exploration. Anchored by a robust Intel Movidius Myriad X Vision Processing Unit and complemented by the Unibap COMExpress e23 family processing core, the system has processing power critical for real-time data analysis and decision-making. Dual Ethernet ports with 10 GbE (10GBASE-T) capability ensure high-speed communication between the satellite and ground station, facilitating seamless command and control operations. This is illustrated as a use case example in Figure 28. Additionally, the inclusion of FPGA DSP cores and OpenCL/HIP GPU accelerators empowers the system to handle complex signal processing tasks and parallel computing challenges inherent in comet surface observation and mining operations.

TABLE XIV
ON-BOARD COMPUTER SPECIFICATIONS

Parameters	Values
RAM	24 GB DDR4 ECC (CPU/GPU)
Storage	2 x 3.8 TB NVMe SSD 1 x 128 GB SATA SSD
Mass	<900 grams
Power	<40 W
Operating System & Software	SpaceCloud OS (Linux)
CoreMark v1.0 per CPU core	25,000+
OpenCL/HIP GPU [GFLOPS]	2000 GFLOP
Additional AI Acceleration	4 TOPS Intel Movidius Myriad X Vision Processing Unit
FPGA DSP cores	924 (18x18)



Fig. 27. On-board Computer: SpaceCloud iX10-101A [22]

It is of crucial consideration that the excess storage does not come at a cost of weight or power consumption penalty, as compared to other Components Off The Shelf (COTS), and provides the freedom and security of saving all the important information until the return of the mission back to Earth. Not to mention that this modular OBGS can be toned down following the user requirements as well, supporting advanced features of mission operations and data processing.

1) Software Architecture:

The software architecture of the OBGS represents a fusion of versatility and adaptability, to facilitate an



Fig. 28. Use Case Example of the selected on-board computer

uninterrupted interplay between hardware components and mission objectives. At its core lies the SpaceCloud Operating System (SCOS/Linux), augmented with advanced computing libraries and AI acceleration capabilities tailored for space-based applications. The SpaceCloud framework provides a standardized API for rapid application development, enabling the deployment of custom algorithms for surface topography mapping using the lidar camera, defined earlier as a use case example in section IV-E on how to carry out computation to determine surface flatness of the comet to evaluate a landing site for ore retriever. Moreover, SCOS's compatibility with third-party tools ensures seamless integration of communication protocols for ground station connectivity and resource management software.

2) Data Processing Algorithms:

The data processing algorithms integrated into the OBGS exemplify its computational efficiency and sophistication, designed to address the unique challenges posed by extraterrestrial mining operations. Leveraging the system's parallel computing capabilities, these algorithms facilitate real-time analysis of lidar camera data to discern the surface topography of the comet, enabling precise navigation and landing of the ore retriever. Furthermore, signal processing algorithms ensure reliable communication with the ground station, facilitating mission control and data telemetry during all phases of the mission.

3) Data Storage Strategy:

The data storage strategy underscores a commitment to robustness, resilience, and data integrity, crucial for the success of long-duration space missions. Leveraging onboard memory modules and fault-tolerant storage protocols, the system ensures the capture and retention of mission-critical data streams, including lidar camera observations, ore composition analyses, and telemetry data. Data redundancy mechanisms and error-checking protocols safeguard against potential data loss during transmission, mitigating the inherent risks associated with deep-space communication. Furthermore, optimized storage formats and compression techniques maximize storage capacity utilization, enabling the efficient archival and retrieval of data for subsequent analysis and processing upon return to Earth.

D. Structural Design [Leo Eitner]

A CAD of the whole spacecraft was modeled using *SOLIDWORKS*, where each subsystem was strategically placed taking into account the thermal and ADCS requirements. Systems that require low temperatures for correct operation like the TT&C and OBCS systems, as well as the cameras, were separated as much as possible from heat sources, like batteries. Symmetry was maintained as much as possible throughout the design to aim for a central of gravity close to the centroid of the satellite. All components of each system were kept together to reduce cable length and transportation losses. Finally, the mission concept of operations was also considered when choosing sensor placement.

1) Materials:

Although not every material of every component was looked at, the main points of interest from the structures' point of view were studied and a suitable material was chosen regarding their specific function.

- **Airframe:** the airframe of the satellite was designed using a grid-like structure as shown in Figure 29. This aims to reduce the weight allocated to structures while maintaining a strong and resistant frame to resist launch, rendezvous, and thrust impulses.

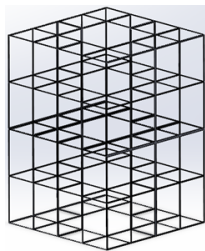


Fig. 29. Satellite airframe.

The chosen material was aluminum 7075, a cheap, common, light but strong alloy ideal for what is required for this mission.

- **Heat Shield:** for the components that are going to be retrieved to Earth, a heat shield is required for them to resist reentry without damage. This is true for the ore container as well as for the OBCS system, which will store valuable data captured during the mission. These will be housed in capsules covered with PICA (phenolic-impregnated carbon ablator), which will be used as an ablative heat shield capable of dissipating almost all the heat generated during reentry.
- **Radiation Shield:** while outside of a protective magnetic field, be it Earth's or any other planet's, the radiation levels are especially high. Although all the space-proven components are already, to some extent, resistant to radiation, the longer the mission time the higher the

probability of radiation-provoked failures. For this reason, the satellite will be enveloped in a thin layer of BPE (Boronated Polyethylene) adding radiation protection to all its components.

2) Mechanisms:

To allow such a big spacecraft to be deployed into Space, coming from a tight and contracted launcher configuration to a deployed and operational state, several mechanisms are required. However, the low reliability of moving parts in Space was considered when designing these mechanisms, and their number was kept to a minimum due to this.

- **Solar panel deployment mechanism:** used to deploy the main module solar panels. Each side contains a 2 DOF (degree-of-freedom) joint that allows the solar panels to rotate ninety degrees once when deployed at the beginning of the mission (spring-loaded and released with pyrotechnical charges) and 360 degrees throughout the whole mission for maximum solar power usage (servo-controlled). Additionally, two more spring-loaded joints which are released with pyrotechnical charges are used per side to fully deploy the retracted sides of the solar panels.



Fig. 30. Main module deployed.

- **Ka-band antenna reflector pointing arm:** used to steer the antenna to make sure it is always pointing towards Earth. It is a 3 DOF robotic arm with servo-actuated joints.
- **Ore retriever landing legs:** each of the four legs of the ore retriever will be deployable and retractable using servo-activated joints.
- **Ore container opening/closing mechanism:** the ore container will open once the ore retriever lands on the comet. This door will then function as a ramp for the rover to easily access the top of the container and unload the mined regolith into it. It will be divided into two sections, making up two sides of the ore container when closed. Therefore, two servo-controlled joints will be used to open/close it.
- **Module separation mechanism:** the satellite is composed of three modules which will be separated using pyrobolts.

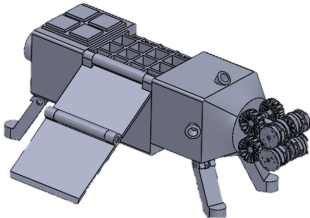


Fig. 31. Ore retriever deployed.

- Module capturing mechanism:** when the ore retriever returns to the main module, a grabbing mechanism will be used to reattach them together. This will be composed of 3 pyro-activated spring-loaded claws which will grab the ore retriever once it slides into its docking compartment.

3) Launcher Compatibility:

As required for every launcher payload deployed into space, it has to be able to resist the harsh conditions during launch. These are a characteristic of every launcher and can be found in their users guide [1]. For SpaceX's Starship, every component of the satellite must be able to resist the following conditions to ensure launcher compatibility:

- Acoustics:** 137.7 dB of OASPL (overall sound pressure level)
- Loads:** 6 g
- Shock:** 1000 g at 1000 Hz

4) Mass and Volume Budget:

With all the components defined it was possible to do a complete mass budget. As Starship will only be able to take 21 tons of payload to GTO, that was the maximum mass limit. For components whose mass could be found, an estimate was made based on other missions. Table XV summarizes the results.

The volume of the spacecraft was derived from the maximum allowed by Starship [1], using cuboids instead of spheroids due to the practicality of having flat faces for component placement and integration. The resulting total volume can be seen in Table XVI.

E. Propulsion Subsystem [Leo Eitner]

When it comes to choosing an adequate propulsion system for a mission, a very extensive study has to be made between

TABLE XV
MASS BUDGET

Subsystem	Component	Quantity	Total Mass [kg]
Propulsion	Main Thrusters	7	31,71
	Propellant Tanks	4	340,46
	Pressuring Tanks	2	49,32
	Lines and Valves	1	9,06
ADCS	Gyroscope	1	8,00
	CMG	4	38
	Sun sensors	5	1,65
	Star trackers	3	3,55
	Attitude Thrusters	24	10,90
Power	Solar Arrays	2	115,40
	Solar Array Drive	2	4,60
	Power Control Unit	1	4,05
	Wiring	1	180,00
	Battery	1	33,00
Thermal	Radioisotope heater	100	3,40
	MLI	1	0,50
OBCS	SpaceCloud Computer	2	1,80
Structure	Main Module	1	393,08
Payload	Camera	1	1,00
	LIDAR	1	7,00
	IR camera	1	4,46
	RASSOR	1	67,00
	Ore Retriever	1	258,62
TT&C	Reflector	1	4,97
	Ka Antenna	1	0,57
	X Antenna	1	0,02
	X Transceiver	1	0,20
	X Transponder	1	3,20
	Ka Transmitter	1	2,27
Total Dry Mass		1378	
Propellant Mass		13300	
Total Wet Mass		14678	
Observation Module		6000	
Total Mass		20678	

TABLE XVI
SIMPLIFIED VOLUME BUDGET

Module	Shape	Volume [m ³]
Main Module	parallelepiped	256
Observation Module	frustum of a square pyramid	163
Total		419

the many available options on the market. To do that, various extensive trade-offs were made.

1) Electrical Propulsion:

An initial study was conducted where electrical propulsion was considered as the principal propulsion system of the spacecraft, as the secondary propulsion system, and with both functions.

- Main engine:** When considering an electrical thruster as the main engine for the spacecraft, the main challenge was the time required to achieve the required orbits. The Ariane Group RIT 2X radiofrequency ion thruster and the Aerojet Rocketdyne AEPS hall thruster were considered for this study. In both cases, the time required to get to the comet's orbit and back would exceed the thruster's lifetime. This problem would also extend to many other

spacecraft components like batteries. Additionally, operation costs would rise proportionally to the mission duration. For these reasons, this option was discarded.

- ADCS Thrusters:** A search for a COTS small electrical propulsion thruster was done to analyze the possibility of using electrical propulsion as the secondary propulsion system. Options such as the Enpulsion Micro, and the Benchmark Space Systems' Xantis Metal Plasma Thruster were found. However, these are designed for microsatellites to serve as their main thruster. They were discarded as they were developed for long-duration burns instead of the short ones required for attitude control, which will be the main function of the thrusters. Additionally, their weight is also superior to the one of a chemical thruster, which makes them even less attractive.

2) First trade-off:

This trade-off aims to evaluate different types of propellants for the propulsion subsystem.

The criteria for this process were established after the studies on propellant selection methods proposed by V.Bombelli et al. [26] and O. Frota et al. [8]. Only the most relevant criteria were considered, listed in Table XVIII. To account for the relevance of the different criteria, weights were introduced. Three different bipropellants were selected as possible candidates, listed in Table XVII.

The MMX mission from JAXA was taken as a reference for this trade-off. For this reason, 4 engines and 20 thrusters were considered for every case [6].

TABLE XVII
TYPES OF PROPELLANT

	MMH/NTO	Ethanol/H ₂ O ₂	Propylene/N ₂ O
ρ_{ox} [kg/m ³]	1448	1390 ¹	1220 ²
ρ_{fu} [kg/m ³]	878	789	611 ²

¹At 20°C. ²At the boiling temperature.

- MMH/NTO:** The S400-15 model from Ariane Group was chosen for the main engines. For the thrusters, the R-6D model from Aerojet company was selected.
- Ethanol/H₂O₂:** No COTS options were found, therefore design parameters for the main engines are based on W.P.W. Wieling et. al. [27]. The thrusters were chosen to be the Halcyon from Benchmark Space Systems.
- Propene/N₂O:** Again, no COTS engine was found and the software Rocket Propulsion Analysis was used instead to simulate the propellants' performance. Values for the chamber pressure and thrust were assumed to be the average between the other two configurations. The B20 thruster from Dawn Aerospace was considered.

After an in-depth analysis of each one of the criteria, a grade between 1 (worst) and 3 (best) was given to each propellant combination. This grade was then multiplied by its respective weight and the final grade was the sum of the weighted grades. Table XIX shows the results.

TABLE XIX
FIRST TRADE-OFF RESULTS.

Criteria	MMH/NTO	Ethanol/H ₂ O ₂	Propene/N ₂ O
Pro. sys. mass	3	3	2
Pro. sys. volume	3	2	1
Mat. compatibility	2	1	2
Hazards	1	3	3
Storability	3	2	1
Ignition	3	2	1
Cost	1	2	3
TRL	3	2	2
Final Grade	3,075	2,625	2,175

3) Second Trade-Off:

As the winner from the first trade-off was the MMH/NTO propellant combination, a second trade-off was conducted to study more in-depth different COTS main engine/thruster combinations that use hydrazine-base propellants. A total of six combinations were composed.

- Medium Thrust MMH/NTO:** S400-15 from Ariane Group/ R-6D from Aerojet Rocketdyne.
- High Thrust MMH/NTO:** R-42 from Aerojet Rocketdyne / R-6D from Aerojet Rocketdyne.
- Medium Thrust MMH/MON:** R-4D-15 HiPAT from Aerojet Rocketdyne / DST-12 from Moog
- High Thrust MMH/MON:** LEROS 4 from Nammo / DST-12 from Moog
- Medium Thrust MMH/MON:** LEROS 2b from Nammo / DST-12 from Moog

TABLE XVIII
CRITERIA AND WEIGHTS

Criteria	Weight [%]
Propulsion System Total Mass	25
Propulsion System Volume	20
Material Compatibility	12,5
Hazards	10
Storability	12,5
Ignition & Combustion	10
Cost	10
Technological Readiness	20

6) **Medium Thrust Hydrazine/MON:** 450N Thruster from IHI Aerospace / 22N Thruster from IHI Aerospace

As done before, the methods proposed by V.Bombelli et al. [26] and O. Frota et al. [8] were taken into account. Due to the similarity between propellant combinations, different criteria and consequently different weights were used in this trade-off.

Finally, in contrast to what was done in the first trade-off, a similar thrust/weight ratio to the MMX mission was aimed for. This value is around 0.05 for MMX. To achieve the same value, 7 main engines were considered for the high thrust configurations and 14 for the low thrust ones.

The new trade-off criteria together with the weights can be seen in Table XX.

TABLE XX
CRITERIA AND WEIGHTS

Criteria	Weight [%]
Propulsion System Total Mass	25
Propellant Volume	20
Tank Similarity	10
Heritage	25
Reliability	20

Again, a grading from 1 (worst) to 6 (best) was given to every criterion and this was then multiplied by its respective weight. The winner of this trade-off was configuration 2, as shown in Table XXI, and the corresponding main engine/thruster combination was used for this mission.

TABLE XXI
SECOND TRADE-OFF RESULTS.

Configurations	1	2	3	4	5	6
Prop. sys. mass	5	6	3	4	2	1
Prop. volume	5	6	3	4	2	1
Tank similarity	6	6	6	6	5	4
Heritage	4	5	5	3	6	5
Reliability	3	6	3	6	3	3
Total	4,35	5,75	3,6	4,35	3,15	2,7

The total required propellant mass, m_p , and volume were computed with the Tsiolkovsky equation (Equation 22). The value used for the wet mass was the maximum allowed value for the main module ($m_0 = 15$ t) and for the ΔV requirements, 6 km/s for the main engines from Orbit subsection IV-C, and 0,5 km/s for the thrusters from ADCS subsection V-B. The final obtained values can be seen in Table XXII.

$$m_p = m_0 \cdot \left(1 - e^{-\frac{\Delta v}{T_{sp} \cdot g_0}}\right) \quad (22)$$

TABLE XXII
TOTAL PROPELLANT REQUIRED.

Propellant	Mass [t]	Volume [m ³]
Oxidizer	8,269	5,73
Fuel	5,034	5,71
Total	13,3	11,44

F. Power System [Anibal Guerrero]

The spacecraft's power subsystem plays a critical role in ensuring the success of the mission by providing the required power to all onboard systems. It is responsible for generating, storing, and distributing electrical energy throughout the spacecraft. Due to the harsh environment of space, where sunlight, temperature variations, and radiation can pose significant challenges. Thus, the design and operation of the power subsystem must be carefully engineered to meet the mission objectives, while ensuring reliability and longevity.

1) Power Budget:

The power budget includes all the power requirements by the different subsystems onboard. It is a crucial aspect, as a careful estimation and management of power consumption will ensure sufficient energy is available in the different cases the spacecraft will encounter throughout the mission.

In this case, the vast amount of the mission will be spent traveling to and from the comet. Additionally, the comet has a size of 0,55km. This infers that eclipses are not a concern. Additional calculations on eclipse times shall be considered in later stages of the mission planning. For now, a system margin of 10% is considered as a conservative approach due to uncertainties and the mission being in its early stages. Table XXIII collects all values for each subsystem and subcomponent of each respectively.

2) Trade-Off & Requirements:

Typically, there are four types of power sources for spacecraft. *Photovoltaic* solar cells, which are the most common source, convert incident solar radiation directly to electrical energy. *Static power* sources use a heat source, typically plutonium-238 or uranium-235 (nuclear reactor), for direct thermal-to-electric conversion. *Dynamic* power sources also use a heater source, typically concentrated solar radiation, plutonium-238, or enriched uranium. These sources convert power using the Brayton, Stirling, or Rankine cycles. The last power source is the *fuel cell*, which is normally used on manned space missions. Table XXXIII provides a comparison of various power sources.

Due to volume constraints, technology, fuel availability, and reliability, a solar photovoltaic is chosen as the power source.

TABLE XXIII
POWER BUDGET

Subsystem	Component	Power (W)
ADCS	Gyroscope	25
	CMG	30
	Sun sensors x 5	1
	Star trackers x 3	8.9
Power	Solar Array Drive Assembly	0.5
	Power Control Unit	1.25
OBCS		7
Payload	Camera	0.9
	LIDAR	40
	IR camera	9.9
	RASSOR	16.42
TT&C	X Transceiver	16
	X Transponder	15.8
	Ka Transmitter	47
Total Power Requirement		219.67
System Margin (SM)		10%
Total Power Requirement with SM		239.67

In comparison, solar cells are cheaper and non-hazardous in comparison to radioisotopes [11].

3) Solar Arrays:

The process of determining the solar array specification requirements for our mission involves several steps, as outlined below:

- 1) Determine requirements and constraints for power subsystem solar array design.
- 2) Calculate amount of power that must be produced by the solar arrays.
- 3) Select type of solar cell and estimate power output.
- 4) Determine the beginning-of-life (BOL) power production capability per unit area of the array.
- 5) Determine the end-of-life (EOL) power production capability for the solar array.
- 6) Estimate the solar array area required.
- 7) Estimate the mass of the solar array.

In designing a solar array, a trade off between mass, area, cost, and risk must be performed. Though silicon presently costs the least for most photovoltaic applications, it often requires larger area arrays and more mass than the more costly gallium arsenide cells. Higher masses and solar array volumes may inquire critical issues down the line, allowing for higher costs or technical risks. Therefore, **gallium arsenide** is chosen as the cell type for the solar arrays.

To estimate the solar array area required for the spacecraft, the power requirement, P_{sa} , must be calculated using Equation 23.

$$P_{sa} = \frac{\left(\frac{P_e T_e}{X_e} + \frac{P_d T_d}{X_d} \right)}{T_d} \quad (23)$$

Where,

$$P_0 = \phi_{sun} * \eta_{array} * F_p \quad (24)$$

P_0 is the power output, ϕ_{sun} is the sunlight flux, η_{array} is the array efficiency, and F_p is the packing factor. The sunlight flux is varying throughout the mission, as the spacecraft will travel to the comet and back. Therefore, an average value of $124.04 W/m^2$ is selected, as the sunlight flux at the average distance throughout the mission. The array efficiency is selected from Table XXIV.

TABLE XXIV
SOLAR CELL EFFICIENCY

Cell Type	Silicon	Thin Sheet Amorphous Si	Gallium Arsenide
Planar Cell	20.80%	12.00%	23.50%
Theoretical Efficiency			
Achieved Efficiency (Production)	14.80%	5.00%	18.50%
Achieved Efficiency (best Laboratory)	20.80%	10.00%	21.80%

$$P_{BOL} = P_0 I_d \cos(\theta_{Sun}) \quad (25)$$

An assembled solar array is less efficient than single cells due to design inefficiencies, shadowing, and temperature variations, collectively referred to as inherent degradation, I_d . With the degradation, and an estimated angle between the array normal and sun rays of 0 ± 5 deg, the beginning-of-life power production capability is calculated (P_{BOL}) in Equation 25. Assuming an annual degradation, a_d of 2.75% intrinsic to these solar cells, the end-of-life power production capability is calculated in Equation 27.

$$P_{EOL} = P_{BOL} L_d \quad (26)$$

$$L_d = (1 - a_d)^{t_{mission}} \quad (27)$$

From the required power the array has to provide, the solar array area, A_{sa} , required to support the spacecraft's power requirement is expressed in Equation 28.

$$A_{sa} = P_{sa} / P_{EOL} \quad (28)$$

The resulting array area for the spacecraft is $84 m^2$. In reality, solar array sizing is more difficult than it appears from theory. This is due to a variation in geometry, angle of incidence on the array surface, and therefore means that either a constant determination of it must be performed, or the calculation of the worst-case angle is needed to develop the P_{EOL} .

4) Battery:

As the spacecraft uses photovoltaics as a power source, it requires a system to store energy for peak-power demands and eclipse periods. Energy storage typically occurs in a battery.

A battery consists of individual cells connected in series. The number of cells required is determined by the bus-voltage. The amount of energy stored within the battery is the Wh capacity. Additionally, batteries can be connected in series to increase the voltage or in parallel to increase the current output. Batteries are split into primary and secondary batteries, where only secondary batteries are rechargeable. For this reason, a secondary battery is selected.

However, there are many options to select from within secondary batteries. For this spacecraft, a Lithium-ion battery is selected for the following reasons:

- Lithium-ion battery technology offers significant advantages over traditional battery types like Nickel-Cadmium (NiCd) and Nickel-Hydrogen (NiH₂) in terms of energy density and operating temperature range.
- The nominal operating voltage for a lithium-ion cell (3.6 to 3.9 Vdc) allows for a reduction in the number of cells required compared to NiCd or NiH₂ cells, resulting in reduced mass and volume for aerospace applications.
- Lithium-ion batteries provide a 65-70% volume advantage and a 50% mass advantage over traditional NiCd and NiH₂ batteries.
- Typical cell constituents of lithium-ion batteries include lithium thionyl chloride, lithium sulfur dioxide, and lithium carbon monofluoride, which contribute to their higher energy density and wider operating temperature range.
- Lithium-ion battery technology is under development and offers specific energy densities ranging from 70 to 110 Wh/kg, making them a promising choice for aerospace applications where higher energy densities are desirable.

The required battery's operational capacity can be calculated according to Equation 29 by using the required power during eclipse $P_{Eclipse}$, eclipse duration $t_{Eclipse}$ and the depth of discharge, DOD , of the battery.

$$C_{bat} = \frac{P_E t_E}{60 \times 60} \frac{100}{DOD} \quad (29)$$

5) Final Characteristics:

To comply with the power requirement, two deployable solar array wings manufactured by DHV are selected [5]. The arrays fulfill the power requirements and each wing deploys to 3 panels, each with a dimension of 1000 × 3039mm, as illustrated in Figure 32. Additionally, and as previously

mentioned, calculating the real power requirement is more complex than applying a set of theoretical equations, even if values obtained through practical experimentation are used for variables such as efficiencies. Therefore, the solar array dimensioning and capabilities must take into account a margin, to compensate for. The rest of the relevant characteristics of the solar arrays are collected in Table XXV.

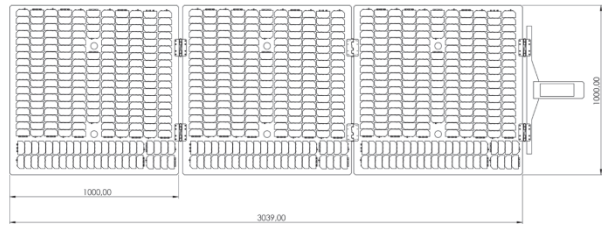


Fig. 32. Solar array dimensions, as provided by DHV [5].

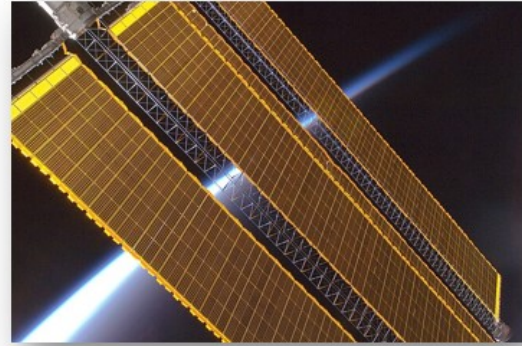


Fig. 33. Representation of 3 unfolded solar arrays, as provided by DHV [5].

For the battery selection, the COTS option shall be Li-ion, shall survive for at least the mission lifetime, which corresponds to 27,000 cycles, and shall have the minimum capacity of 966.7Wh. Therefore, a *ibeos B28-1100 Satellite Battery* is selected [20]. The rest of the relevant characteristics of the battery are collected in Table XXV.

TABLE XXV
FINAL BATTERY & SOLAR ARRAY CHARACTERISTICS

Component	Property	Value	Unit	Solution Values
Battery	Operational Capacity	966.7	Wh	1,100
	DOD	30	%	30
	Lifespan	27,000	Cycles	40,000
	Battery Type	Li-ion	-	Li-ion
Solar Array	Power BOL	488.92	W	1000
	Power EOL	437.45	W	-
	Degradation	-2.75	%/year	-
	Area	84	m ²	2 x (3x7.5x2) = 135
	Incidence Angle	0	°	-

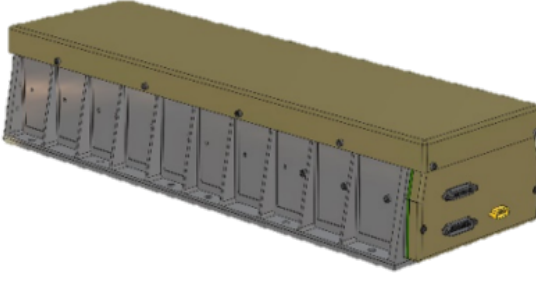


Fig. 34. ibeos B28-1100 Satellite Battery [20].

G. Thermal Control [Alessandro Tinucci]

Another important aspect in the design of a spacecraft is Thermal Control, ensuring that all instruments are within their operational range of temperatures and are able to function without issues.

For this, a set of simulations were carried out to validate our system using the Simscape tool embedded in MATLAB. This was also incorporated into the GMATLAB framework, where the Montecarlo simulation checked, for a whole spectrum of configurations of power, orbits and the rest of the subsystems, that the minimum and maximum temperatures experienced were at acceptable levels.

The many unknowns left free by the preliminary design phase this whole project consists of means the precise elaboration of a system that accurately depicts the thermal behavior of the spacecraft is not an easy task.

In the picture below a schematic of what the system model inside of Simscape looks like can be seen,

Three blocks regarding the physical model can be differentiated, namely the environment, losses and spacecraft systems.

In the spacecraft system, the most important of them all, the simplifications made can be observed. A big component representing the entirety of the spacecraft with the corresponding thermal inertia is the main body to which the critical instruments of which we wanted to simulate the thermal behavior of are attached. These instruments are the on-board computer system, and two cameras.

Their thermal influence was been modeled as a heat flow rate source, heating the main body through thermal conduction and through the respective resistances that model the existing structural connections existing in the system.

The effect of the environment was modeled in its respective block where a day-night cycle was also implemented in order to simulate a worst-case scenario caused by eclipses. In that block the radiative heating of the sun was modeled as an oscillatory step function that continually turned on and off (10 percent of the orbit time was considered to be in total penumbra) the magnitude of the heat flow generated by the sun.

Experimenting with different modulations of the heat generated by the sun to better reflect the dimming happening as the

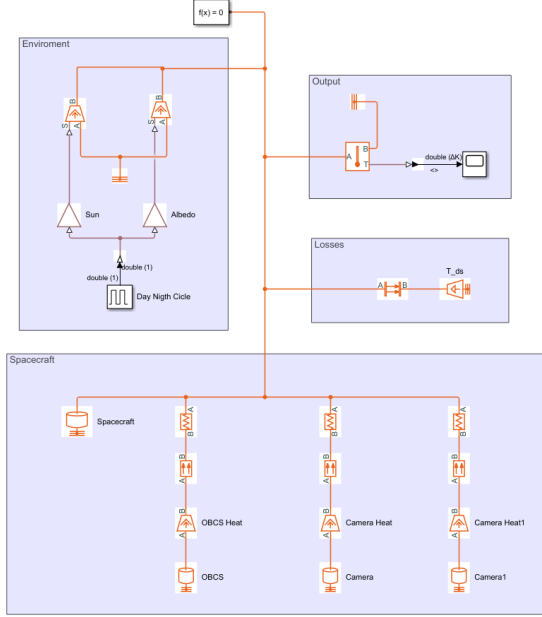


Fig. 35. Spacecraft's thermal model in Simscape.

sun rises up and lowers over the horizon might be of interest. Additionally, radiation losses were also modeled in the losses block.

With that, the output obtained for the temperature experienced by the spacecraft can be seen here,

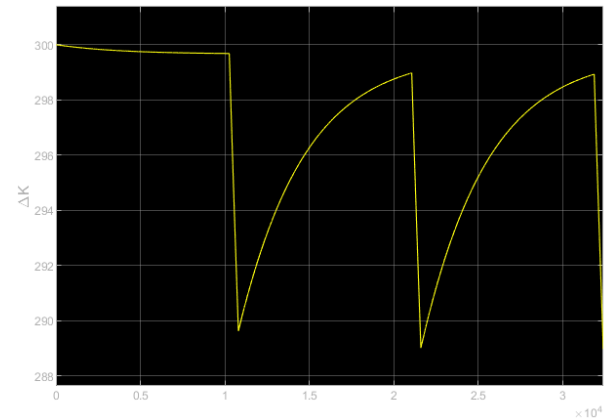


Fig. 36. Spacecraft's temperature fluctuations.

This plot very graphically represents the different phenomena happening during the thermal cycles. First of all, it can be seen that the temperature range is very well withing the operational range.

But it also perfectly captures the nonlinear decrease in temperature after the sun occludes behind the comet, due to the body's thermal inertia. And also the progressive heating up once the sun appears again. Finally, it can be observed the decreasing tendency of the peaks of temperature after each

night-day cycle, showing the stabilization of the system as it approaches equilibrium.

The final solutions that were adopted to ensure the thermal stability of the system were two, one active and one passive. The active one consists in a 7W electric heater used during the cold phases to increase the temperature of the critical components. The passive one consists in a multi-layer mylar insulation, that helps decrease the fluctuations of temperature decreasing losses in the system.

VI. PAYLOAD INTEGRATION

A. Mechanical Integration [Leo Eitner]

As there are two different types of payload integrated into the spacecraft, this section is divided into two: optical payload and rover mechanical integration.

1) Optical Payload:

- **Mounting and Attachment:** The optical sensors will be securely mounted onto the satellite's structure using precision mounting brackets to ensure a stable and vibration-resistant connection.
- **Structural Compatibility:** They will be designed to be compatible with the satellite, ensuring they withstand mechanical loads during launch and maintain precise alignment for imaging operations.
- **Thermal Considerations:** Thermal insulation will be incorporated to protect the optical components from extreme temperature variations. Additionally, they will be actively heated when necessary.
- **Vibration and Shock Analysis:** Vibration and shock analyses have to be conducted to ensure their resilience to launch-induced shocks and vibrations.
- **Spacecraft Bus Interaction:** All optical sensors will interface with the spacecraft's bus to receive power, commands, and transmit data. This means the payload has to be connected to the satellite's power distribution system and data communication network.
- **Alignment and Calibration:** Precise alignment procedures have to be conducted to ensure accurate pointing. These have to certify the correct performance under the many conditions expected during the mission.
- **Integration Testing:** Comprehensive integration tests such as image acquisition, data transfer, and response to different operational scenarios must be performed to validate the functionality of the optical payload within the satellite system.

2) Rover:

- **Mounting and Attachment:** The rover and all its subsystems, which include mobility systems, scientific instruments, and communication devices, are securely mounted onto the ore retriever bus. Mounting points must be designed for stability during launch, module separation, and landing.
- **Structural Compatibility:** The rover is structurally compatible with the satellite bus, ensuring that it can withstand the mechanical stresses encountered during launch, module separation, and landing.
- **Thermal Considerations:** Thermal protection is integrated to shield the rover from extreme temperature conditions while it is inactive and can't use its thermal regulation system. This will be done with heaters and MLI.
- **Vibration and Shock Analysis:** Vibration and shock analyses must be conducted to assess the impact of

launch, landing, and module separation on the rover's components.

- **Spacecraft Bus Interaction:** The rover interfaces with the spacecraft's communication system for sending TT&C data back to the Ore Retriever / Main Module. Integration involves establishing reliable communication links between them.
- **Alignment and Calibration:** Alignment procedures must be implemented to ensure proper alignment of the rover with the Main Module to ensure smooth separation of the ore retriever from the main body.
- **Integration Testing:** Extensive integration tests will be performed to validate the rover's functionality after experiencing all the environments it is expected to be subjected to before being deployed. This includes testing of instrument deployments, communication systems, and autonomous navigation.

B. Electrical Integration [Anibal Guerrero]

The electrical integration of the spacecraft involves the integration of various electrical components and systems to ensure that they work together throughout the entire mission. This process includes integrating power generation, distribution, storage, and management systems, as well as communication, navigation, and payload systems.

One of the key considerations during electrical integration is ensuring that different subsystems and components are compatible and work well together. This requires careful planning and coordination to avoid conflicts. For example, power generation systems like solar arrays need to be integrated with power distribution and storage systems to provide a steady and reliable power supply to all spacecraft subsystems.

Electrical integration also involves designing and installing wiring and harnesses to connect various electrical components and subsystems. This includes routing cables, harnesses, and connectors throughout the spacecraft structure while considering factors like electromagnetic interference (EMI), thermal management, and structural integrity. For example, the rule of thumb to calculate the total mass of wiring through the whole spacecraft is estimating its mass as 4% of the total mass of the spacecraft. Additionally, a Power Control Unit (PCU) is necessary to control the power flow from the solar arrays to the payload cameras, subsystems, and the battery. Additionally, they are also responsible for regulating, and monitoring.

PCUs incorporate fault detection mechanisms to monitor electrical power abnormalities such as overloads, short circuits, or voltage spikes. In the event of a fault, PCUs activate protective measures such as isolating affected circuits or shutting down to prevent further damage to the spacecraft.

Furthermore, PCUs prioritize power allocation during critical mission phases and adjust power distribution as needed to optimize spacecraft performance.

In addition to hardware integration, software integration is also crucial. This entails programming and configuring onboard computers, processors, and controllers to effectively manage and control the spacecraft's electrical systems, as mentioned in subsection VI-C. It also involves developing and testing communication protocols, data interfaces, and command and control systems to ensure smooth communication between the spacecraft and ground control.

For preliminary designs, going very in-depth into electrical integration is a complex process that requires careful planning and many iterations, coordination, and testing to ensure the spacecraft operates effectively and achieves its mission objectives.

C. Software Integration [Sibtain Ali]

For any space mission, the software integration process serves as the conductor, orchestrating seamless collaboration between the On-Board Computing System (OBCS) and vital subsystems essential for mission success. Leveraging the robust hardware capabilities of the OBCS subsystem as detailed in section V-C, it allows to implement algorithms that interface with key systems such as the Attitude Determination and Control System (ADCS), Tracking, Telemetry, and Command (TT&C), as well as power and thermal management subsystems. Through the built-in software modules, the OBCS interfaces with the ADCS to execute precise maneuvers, ensuring optimal positioning of the satellite for observation and communication while also facilitating the descent and ascent of the ore retriever to and from the comet's surface. This integration enables the OBCS to dynamically adjust spacecraft orientation and trajectory in response to real-time telemetry data, ensuring efficient resource utilization and mission safety.

Furthermore, the software integration efforts extend to the TT&C subsystem, where the OBCS serves as the central nervous system, coordinating communication between the satellite and ground control. Utilizing advanced communication protocols and error-checking algorithms, it manages data transmission, telemetry feedback, and command reception, enabling seamless command execution and data exchange with the ground station. Moreover, the collaboration with power and thermal management subsystems helps to optimize onboard resources, balancing computational demands with power consumption and regulating temperatures to safeguard hardware integrity. By harmonizing the functionalities of these critical subsystems through software integration, the OBCS ensures mission reliability, resilience, and operational efficiency, throughout the mission lifecycle.

VII. LAUNCH & DEPLOYMENT

A. Launch Strategy [Anibal Guerrero]

This mission aims to utilize the capabilities of the Starship to achieve a Geostationary Transfer Orbit (GTO). GTO allows for efficient transfer of payloads, providing the necessary altitude and inclination for the spacecraft to escape Earth's orbit and go interplanetary.

By leveraging the performance and flexibility of the Starship, reliable and cost-effective access to space for this mission is ensured. The fully reusable nature of the Starship also contributes to reducing launch costs and increasing accessibility to space.

The launch strategy consists of launching with the Starship from SpaceX's Starbase in Texas. An illustration of a Starship mounted onto the launch tower at Starbase is represented in Figure 37.



Fig. 37. SpaceX's Starship mounted to their launch tower at Starbase, TX.

TABLE XXVI
TECHNICAL INFORMATION ON LAUNCH OPPORTUNITY.

Parameter	Value	Unit
Operator	SpaceX	-
Launcher	Starship	-
Launch Location	Starbase, TX, US	-
Orbit	GTO	-
Available Payload	21	t
Latitude	25.59	°

As the spacecraft considered for this mission is composed of several modules, but designed to fit inside Starship's fairing volume and weight constraints, a single launch is required to fully deploy all relevant components of the mission. Further information on the structural considerations and integration can be consulted in subsection V-D and subsection VI-A,

respectively.

B. Deployment Sequence [Leo Eitner]

The deployment sequence of the whole satellite can be described in the following order of steps:

- 1) **Launcher separation:** once the launcher reaches GTO, the satellite is deployed into orbit.
- 2) **Detumbling:** the satellite uses its ADCS system to stabilize its attitude.
- 3) **Solar array deployment:** once stabilized, the solar panels are deployed and all power-dependent subsystems are activated for status checks.
- 4) **Antenna deployment and communication:** the antenna reflector will be deployed and pointing tests will be done. Communication using both the X and the Ka-band antennas will be tested.
- 5) **Health check and telemetry:** the spacecraft will communicate with the ground and provide information about the state of each subsystem.
- 6) **Hold:** the spacecraft will await a command from the ground station to proceed with the mission if everything looks nominal.
- 7) **Escape burn:** if every subsystem is working properly, the spacecraft waits for its next perigee to perform an insertion burn into the desired transplanetary orbit to the MBC.

VIII. MISSION OPERATIONS [LEO EITNER]

A. Ground Station Design

To communicate with Earth, the spacecraft will use the Deep Space Network (DSN). A network of ground stations positioned in strategic points around the globe to ensure at least one of the ground stations is always reachable from any point in Space.

Although expensive, this network is specially designed for deep Space communication, as each ground station contains multiple 30+ meter antennas that communicate in every Space application radio frequency band, and have some of the most sensible receivers and powerful transmitters available.

For this mission, the MM will use the 34-meter antennas to communicate in the X-band, both downlink and uplink and the 70-meter antennas to communicate in the Ka-band, only downlink.

B. Communication Windows

The communication windows depend on the ground station selected, the eclipse time of the body the spacecraft is orbiting, and, when orbiting bodies besides Earth and the Moon, the relation between Earth's orbit and the orbit of the body being orbited.

As mentioned in the previous subsection, there will be no gaps in the communication due to the ground station being out of reach, as there will always be one accessible within the DSN. There might be communication outages in the Ka-band due to bad atmospheric conditions, but the X-band communication is immune to them.

Regarding relative positioning between bodies, no communication is possible when the Sun or any other inner Solar system body is obstructing the link. Due to simplicity and relevance, only the Sun case was considered. A diagram representing the assumptions considered can be seen in Figure 38. With it, Equations 30 to 33 were used to compute the amount of time per year in which the Sun covers the Earth, t_s .

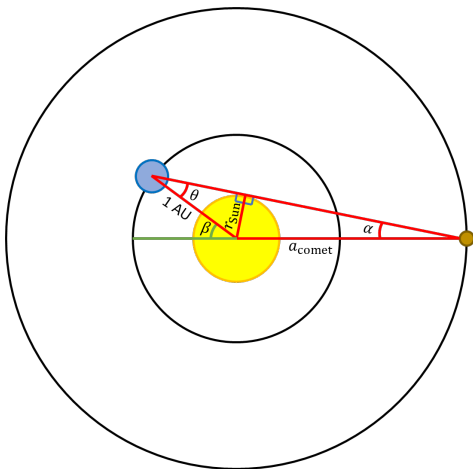


Fig. 38. Communication outages diagram.

$$\alpha = \arcsin \left(\frac{r_{Sun}}{a_{comet}} \right) \quad (30)$$

$$\theta = \arcsin \left(\frac{r_{Sun}}{1AU} \right) \quad (31)$$

$$\beta = \theta + \alpha \quad (32)$$

$$t_s = \frac{2\beta}{360^\circ} \times 1\text{year} \approx 17\text{ h } 9\text{ min} \quad (33)$$

The eclipse time, although not computed, was assumed to be the same as the Sun's eclipse time, that is 10% of the orbit's period. This is a conservative approach, as the short orbit period combined with the asteroid's small size makes the time the spacecraft spends in its communication shadow nearly zero. Additionally, orbit inclination also plays a big role. With this value it is assumed the worst case scenario, that is, the spacecraft is always orbiting in the ecliptic plane, and therefore, always experiences the longest possible eclipse time.

In the end, the total time, per year, in which the spacecraft can communicate with Earth, t_{com} , was computed with Equation 34.

$$t_{com} = (1\text{year} - t_s) \times 90\% \approx 328\text{ days} \quad (34)$$

C. Expected Data Volume

The expected data rate of the overall communication can be seen in Table XXVII. The data rate for TT&C was taken from the usual values for deep Space missions, while the data rate for the science data was computed taking into account the capacity and modulation of the chosen transmitter, the maximum allowable antenna reflector size (8 m), and the minimum E_b/N_0 required for error-free communication ($\text{BER} < 10^{-5}$).

TABLE XXVII
EXPECTED DATA RATES

Function	Bit rate [bps]
Command	64 [12]
Health & Status Telemetry	100 [12]
Science Data	4 000
Total (Br _{total})	4 164

The expected yearly data volume, V_{data} can now be computed with Equation 35.

$$V_{data} = t_{com} \times Br_{total} \approx 13,7\text{ GB} \quad (35)$$

IX. RISK MANAGEMENT

A. Risk Analysis, Mitigation and Backup [Sibtain Ali]

Table XXVIII details the risk analysis, with classification referring to the severity of the impact of each of them on the overall mission success. The mitigation and backup strategies have been closely linked to the methods already applied in the corresponding subsystems in earlier sections, or similar, therefore not demanding extra technological or economical efforts.

TABLE XXVIII: Risks Analysis, Mitigation and Backup

Risk Identification	Classification	Mitigation	Backup
Navigating the spacecraft through the Main Belt	High	Conduct extensive trajectory simulations and Reliable communication channel	-
Unplanned comet encounter	High	Comet detection algorithms	Emergency trajectory adjustment protocols
Funding instability	High	Diversified funding sources	-
Radiation induced electronic failure	Medium/High	Radiation hardened components	Redundancy
Adverse space weather conditions	Medium	Early warning systems	-
Unforeseen gravitational perturbations in orbit	Low	-	Have reserve propellant for potential ADCS corrections
Weather related launch delays	Low	Calculate launch windows and launch scenarios	Contemplate other launch opportunities
Payload			
Deployment failure of ore retriever	High	Extensive pre-launch testing, ensuring TRL-6	Alternate deployment mechanisms
Optical sensor malfunction/calibration issues	Medium/High	Check for sensors flight heritage and compatibility with mission	Incorporate redundant sensors
Extraction rover mobility on comet	Medium/High	Identification of suitable landing/mining area	-
Limited resource extraction capacity	Low	Equipment and power source redundancy	-
Propulsion			
Leakage may deplete the fuel supply critical to the mission	High	Implement regular fuel level monitoring and detection systems	Pre - Plan for emergency fuel containment procedures; During - Optimize mission trajectory
Anomalies in propulsion system impacting mission course/trajectory	Medium/High	Incorporate redundant propulsion mechanisms and onboard diagnostics	-
Fuel Contamination	Low/Medium	-	-
ADCS			
Drift in sensor calibration may lead to inaccurate attitude determination – especially during ore retriever rendezvous	High	Check for sensors flight heritage and test for performance and calibration	Incorporate redundant sensors with required accuracies

Actuator Failure (thruster misfiring or mechanical fault in momentum exchange devices)	Medium/High	Avoid actuating them to the maximum performance	Incorporate the required number of redundant actuators that can help to complete the mission
Limited Torque generation	Low/Medium	Design the actuators for an extra margin of actuation requirement	-
Sun sensor blind spots	Low	Incorporate sensor fusion, for instance with star trackers	-
OBCS			
Software system corruption	High	Conduct testing of software updates and patches	Auto-recovery system or redundant hardware
Malfunction	Medium/High	Check for flight heritage and compatibility with mission	Have redundant on-board computers on stand-by
Inadequate memory	Low/Medium	Conduct memory management	-
TT&C			
Malfunction of hardware	High	Check for space heritage and performance tests	Redundancy
Telemetry signal dropout	Medium	-	Plan for delayed telemetry data transmission
Limited command uplink reliability	Low/Medium	-	-
Data transmission interference	Low	Implement encryption measures	Have sufficient data storage capabilities
Thermal			
Subsystem failure	High	Monitoring and diagnostics of thermal systems	Design for redundant components – alternative thermal control
Inadequate heat dissipation	Medium	-	Consideration of passive methods
Thermal sensor calibration drift	Low	-	-
Power			
Solar Panel Degradation	High	Performance monitoring of solar panels	-
Power generation variability	Low/Medium	-	Alternate power sources – such as batteries
Structure			
Re-entry overheating	High	Use of insulating materials and structural reinforcements	-
Intensive vibrations during launch	Medium/High	Damping mechanisms and structural reinforcements	-
Thermal Expansion/Contraction	Low/Medium	Active thermal control	-

B. Budget & Cost Analysis [Anibal Guerrero]

To calculate the total cost budget of the mission, three major subcomponents are identified: *launch costs*, *operational costs*, and *spacecraft development costs*.

1) Launch Costs:

The estimated cost for launching payloads into space with Starship for this mission is assumed to be 20 €/kg. However, a more conservative value of 50 €/kg is adopted to ensure adequate budgeting for the project, as companies (especially launchers), tend to exaggerate their estimates to increase expectations of future clients. Nevertheless, this conservative value is still orders of magnitude smaller than any other current launch opportunity payload cost, which will make space more accessible to everybody.

Starship's payload capabilities allow for 150 metric tons to LEO, or 21 metric tons (t) to GTO. Even though this mission's spacecraft concept is beneath the 21t limitation, it is assumed that all weight capabilities are utilised. This assumption roots from the early stage of the mission concept at the current stage, as further considerations end up requiring more mass and volume requirements. Therefore, it is assumed that the *Comet Explorers* launches 21t to GTO.

Theoretically, this would mean that the total cost for the payload launch would be $21t \times 50\text{€}/\text{kg} = 1,050,000\text{€}$. However, there are additional factors that need to be considered. In addition to the base launch cost, other factors such as transportation and assurance are also taken into account. These factors account for a certain percentage of the total launch cost and are essential for ensuring the success and safety of the mission. Typically, transportation to the launch site and assurance are 4%, and 8% respectively, of the initial launch cost estimate. Therefore, the total launch cost estimate taking into account transportation and assurance becomes $1,050,000\text{€} \times 1.12 = 1,176,000\text{€}$. These results are collected in Table XXIX.

TABLE XXIX
LAUNCH COST CALCULATIONS

Parameter	Value	Unit
Payload Cost	50	€/kg
Spacecraft Mass	21	t
Launch Cost	1,050,000	€
Transportation	4	%
Assurance	8	%
Total Launch Cost	1,176,000	€

2) Operational Costs:

The Deep Space Network (DSN) is a worldwide network of antennas that supports interplanetary spacecraft missions,

as well as some Earth-orbiting missions. It is operated by NASA's Jet Propulsion Laboratory (JPL) and plays a critical role in communication with interplanetary spacecraft.

The DSN consists of three main tracking stations strategically located around the globe: *Goldstone*, California; *Canberra*, Australia; and *Madrid*, Spain. These stations are positioned approximately 120 degrees apart, ensuring continuous coverage of spacecraft as the Earth rotates. Each station is equipped with large, highly sensitive antennas that can receive and transmit radio signals to and from spacecraft across vast distances.

The primary functions of the DSN include tracking spacecraft, receiving telemetry data, sending commands to spacecraft, and providing navigation support. By maintaining constant communication with spacecraft, the DSN enables mission operators to monitor the health and status of spacecraft systems, upload software updates, and conduct scientific experiments.

It is crucial to consider the operational costs associated with maintaining communication and tracking capabilities throughout the mission's duration. For this mission, utilization of the DSN is a key components of the operational infrastructure.

When considering the operational costs of using the DSN, there are several factors and assumptions that must be made to estimate the total cost:

- **Estimated Development Duration:** 4 years
 - Estimated time required for the development phase of the mission, which includes designing, building, and testing the spacecraft and its systems.
- **Expected Production Duration:** 1 year
 - Anticipated duration for the production phase of the mission, in which the spacecraft will be manufactured and assembled.
- **Mission Lifetime:** 4 years
 - Planned duration for the entire mission.
- **Hours per Track:** 0.4 hours
 - Amount of time allocated for each communication session between the spacecraft and the DSN.
- **Number of Tracks per Week:** 3 sessions per week
 - Frequency at which the spacecraft will communicate with the DSN, expressed as the number of tracking sessions per week.
- **Number of Weeks Required:** 204 weeks
 - Total duration in weeks needed to complete the communication sessions over the mission's lifetime.
- **Yearly Inflation Rate:** 3.2%
 - Annual percentage increase in costs due to inflation, which affects the overall operational expenses over time.

- **Total Cumulative Inflation Multiplier:** 1.134
 - Factor by which costs increase over the entire mission duration, considering the cumulative effect of annual inflation rates.
- **Non-Government Reimb. Adjustment Factor:** 1.4
 - Adjustment factor applied to account for non-government reimbursement or funding sources that may affect operational costs.
- **Total Time Required:** 856.8 hours
 - Aggregate time needed for all communication sessions between the spacecraft and the DSN throughout the mission.
- **DSN Aperture Cost:** 1,057 k€
 - Cost associated with the aperture (size) of the DSN antennas used for communication with the spacecraft, measured in thousands of Euros (k€).

The operational costs associated with utilizing the Deep Space Network for communication and tracking of the spacecraft are outlined in Table XXX.

TABLE XXX

OPERATIONAL COSTS BREAKDOWN USING THE DEEP SPACE NETWORK,
ASSUMING A CONNECTION 3 DAYS PER WEEK.

Key	Value	Unit
Estimated Development Duration	4	year
Expected Production Duration	1	year
Mission Lifetime	4	year
Hours per Track	0.4	h
Number of Tracks per Week	3	/week
Number of Weeks Required	204	weeks
Yearly Inflation Rate	3.2	%
Total Cumulative Inflation Multiplier	1.134	-
Non-Gov Reimb. Adjustment Factor	1.4	-
Total Time Required	856.8	h
DSN Aperture Cost	1,057	k€
DSN Support Summary		
Total Cost for period Fiscal-Year	3,243,305	€/year
Total Operational Costs	12,973,221	€

3) Development Costs:

To estimate the development costs of the mission, several analogous missions that share similarities with this mission are selected. These missions have been chosen based on their objectives, target destinations, and technical complexity, making them suitable benchmarks for cost estimation.

The selected analogous missions are as follows:

- **Hayabusa2:** JAXA mission aimed to study the asteroid Ryugu and return samples to Earth. Its similarity lies in its goal of sample return from a small body in the solar system.
- **Hayabusa:** Predecessor to Hayabusa2, this mission also targeted an asteroid (Itokawa) for sample return, pro-

viding valuable insights into the challenges and costs associated with such missions.

- **OSIRIS-REx:** Designed to study the asteroid Bennu and return samples to Earth. Like this mission, OSIRIS-REx focuses on a comet/asteroid target and sample return objectives.
- **Deep Impact:** NASA mission involved intentional impact of a spacecraft into comet Tempel 1 to study its composition.
- **Dawn:** NASA mission to explore the asteroid belt, visiting the protoplanet Vesta and the dwarf planet Ceres.
- **Stardust:** Another NASA mission, collected samples from the coma of comet Wild 2 and returned them to Earth. Analogous to this mission, involved the study of cometary material.

Table XXXI contains all development costs for the relevant analogous missions.

TABLE XXXI
DEVELOPMENT COSTS FOR ANALOGOUS MISSIONS & AVERAGE

Analogous Missions	Value	Unit
Hayabusa2	150	M€
Hayabusa	150*	M€
OSIRIS-REx	588.5	M€
Deep Impact	383.4*	M€
Dawn	508*	M€
Stardust	214*	M€
Average Development Cost of Analogous Missions	332.32	M€

Where values marked with * indicate an inflation-adjusted price to 2024.

4) Total Cost Estimation:

TABLE XXXII
TOTAL COSTS OF THE MISSION

Cost	Value	Unit
Launch	1.18	M€
Development	332.32	M€
Operational	12.97	M€
Estimated Total Costs	346.47	M€

The total cost of the mission, as outlined in Table XXXII, encompasses various components crucial for its success.

The launch cost, totaling approximately 1.18M€, represents the expense associated with deploying our spacecraft into space atop the Starship launcher, a future cost-effective option for such missions. These dramatically reduced costs would enable new actors entering the space scene, and technological innovations previously constrained to volume and weight limitations.

Development costs, amounting to 332.32M€, are based on the average of analogous missions' expenses adjusted for

inflation. These costs cover the design, construction, testing, and preparation of our spacecraft and instruments, ensuring they meet the mission's objectives and technical requirements.

Operational costs, estimated at $12.97M\text{€}$, include the expenses associated with utilizing the Deep Space Network (DSN) for communication and tracking purposes. These costs are essential for maintaining regular contact with the spacecraft, monitoring its health, and receiving scientific data throughout the mission's duration.

X. TIMELINE [ANIBAL GUERRERO]

A Gantt Chart is a powerful tool for visualizing the schedule of a project, breaking down tasks and objectives over time. Figure 39 presents the time management plan for the design concept of this mission, depicting various objectives and tasks necessary for the successful execution of it.

The Gantt Chart has allowed for a clear overview of the timeline for each task that is to be completed, allowing for effective planning, coordination, and monitoring of progress. By breaking down the project into manageable components and assigning specific timeframes, it is ensured that all aspects of the mission are addressed in a systematic and timely manner.

Each objective and task shown in the Gantt Chart corresponds to a specific aspect of the mission, such as spacecraft design, and subsystem developments. By following this structured timeline, the execution of the project has been streamlined, to achieve goals efficiently.

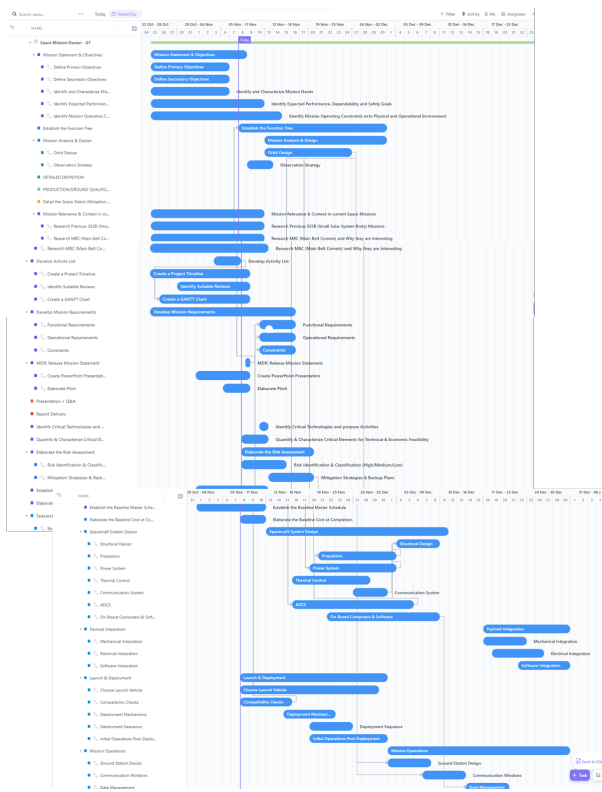


Fig. 39. Time Management for design concept of this mission, subdivided in objectives and tasks.

All project management considerations are carried out in ClickUp. ClickUp is a powerful project management platform designed to streamline and enhance collaboration,

organization, and productivity for teams of all sizes. It offers a wide range of features and functionalities that make it an invaluable tool for managing projects like ours.

At its core, ClickUp provides a centralized hub where team members can access project-related information, communicate effectively, and track progress in real-time. Figure 40 shows a snapshot of how tasks are segmented into requirements for each of the design phases the project moves through. It is essential for task assignment, clarity, and organization. Additionally, one has the ability to define interdependencies with other tasks, and requirements before a task can be started, similarly to how real projects are managed.

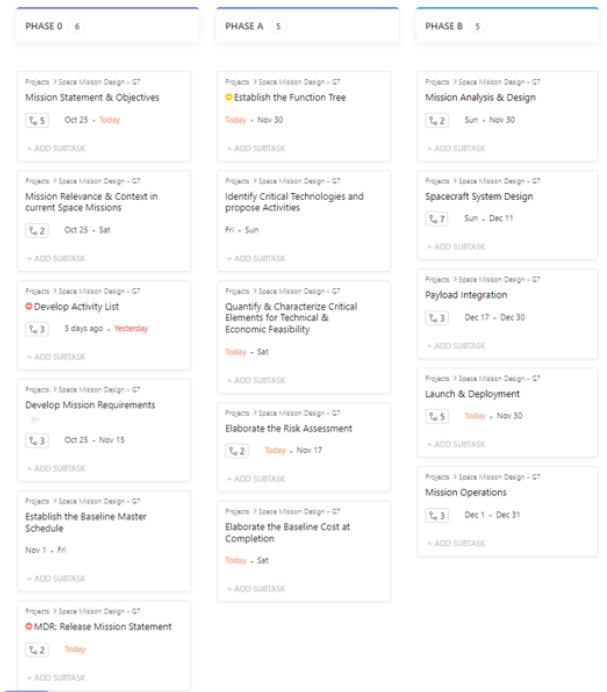


Fig. 40. ClickUp Task assignation example for *Comet Explorers*' mission.

XI. END-OF-LIFE PLANNING

A. Expected Mission Life [Anibal Guerrero]

As explained in subsection IV-C, the mission can be subdivided into phases. In total, it will take ~ 600 days to go from the initial GTO orbit to the comet. Mining activities detailed in subsubsection IV-D2 would take ~ 22 days. The return trip is estimated of an approximate length to the trip to the comet. In total, the mission is estimated to last 1250 days. In future, more developed phases of the mission concept, this timeline will likely be extended, as deployment sequence delays will be considered, as well as more accurate orbit design considerations with respect to the orbit around the comet. Taking a conservative approach of adding a 20% margin, one can estimate the total mission life to be of 1500 days.

B. Deorbiting Strategies [Alessandro Tinucci]

Debris mitigation is crucial for preserving the safety and sustainability of space operations. As the volume of debris in orbit around Earth increases, the risk of collisions with operational satellites and crewed spacecraft also escalates. Such collisions can result in significant damage, potentially rendering vital satellites inoperative and endangering human life in crewed missions.

Although our mission develops in an interplanetary scenario, the plan to return the mined resources to Earth makes deorbiting considerations necessary as well. As already mentioned, this phase of the mission design was considered from the start during the trajectory planning. Even though the complexity of the mission profile made the assumption of some simplifications and the adoption of a purely numerical model for the simulation a necessity.

In particular, an incidence angle with respect to Earth's horizon of around 6 degrees was aimed for. An ablative heat-shield for the reentry and parachutes for the recovery were considered, although the elaboration of a separate study at a more advanced design phase is required.

XII. CONCLUSIONS [EVERYONE]

SpaceX's Starship presents a significant opportunity for reducing mission costs, opening up possibilities for previously untapped mission proposals within the current market landscape. The cost-effectiveness of utilizing the Starship platform enables ambitious space exploration missions to be considered viable.

The feasibility of the *Comet Explorers* mission has been demonstrated through the preliminary design phase. Despite the high complexity and numerous potential challenges identified, the initial study indicates that the mission concept is technically achievable.

However, certain challenges have been identified that require further analysis and optimization in later development stages. One such challenge is the reduced gravitational forces encountered in MBCs and SSSBs, which may impact the functionality of mining equipment and propulsion requirements. Addressing these challenges will be crucial for ensuring the success of the mission.

In-depth analysis and optimization of the interplanetary trajectory are necessary to refine mission planning. This includes considering factors such as the number of burns, gravity assists, and trajectory optimization techniques to optimize the spacecraft's path to the target comet. Similarly, orbital design around the comet requires thorough investigation to determine the most suitable orbit for scientific observations and data collection. This involves studying gravitational conditions around the comet and assessing the feasibility of halo orbits or other orbital configurations such as hovering around equilibrium points, and considering chaotic orbital systems.

Despite these challenges, the *Comet Explorers* mission holds significant scientific value and has the potential to provide crucial insights into fundamental questions regarding the origin of water on Earth. [15]

XIII. APPENDIX

A. Subsystem Level Requirements

A	B	C	D
Category	Module	Subsystem	Description
2 Constraints	ER (Extraction Rover)	PL (Payload)	The payload subsystem shall provide TBD m3 of space for the mining equipment to fit in.
3 Functional	ER (Extraction Rover)	PL (Payload)	The payload subsystem shall collect volatile materials from the surface of the MBC
4 Functional	ER (Extraction Rover)	EP (Electrical Power)	The subsystem shall provide power to extract TBD kg of regolith.
5 Functional	ER (Extraction Rover)	PL (Payload)	The payload subsystem shall be within a volume of TBD m3.
6 Functional	ER (Extraction Rover)	PL (Payload)	The payload subsystem shall weigh less than TBD kg.
7 Functional	ER (Extraction Rover)	PL (Payload)	The payload subsystem shall operate for no longer than TBD hours before the Ore Retriever is launched.
8 Functional	ER (Extraction Rover)	PL (Payload)	The payload subsystem shall implement an anchoring system for stable rover operations during regolith extraction.
9 Functional	ER (Extraction Rover)	EP (Electrical Power)	The power subsystem shall include energy harvesting capabilities, such as solar panels.
10 Operational	ER (Extraction Rover)	ST (Structures)	The structural subsystem shall withstand landing loads on MBC
11 Operational	ER (Extraction Rover)	ADCS (Attitude & Control)	The ADCS subsystem shall be capable of re-orienting the rover once landed.
12 Operational	ER (Extraction Rover)	PL (Payload)	The payload subsystem shall extract TBD kg of regolith.
13 Operational	ER (Extraction Rover)	EP (Electrical Power)	The power subsystem shall integrate battery health monitoring systems to assess the status of power storage units
14 Functional	MM (Main Module)	PROP (Propulsion)	The propulsion subsystem shall have sufficient propellant mass for the entire duration of the mission.
15 Functional	MM (Main Module)	ADCS (Attitude & Control)	The ADCS subsystem shall de-tumble the module at TBD rate
16 Functional	MM (Main Module)	ADCS (Attitude & Control)	The spacecraft shall point towards the MBC with TBD accuracy.
17 Functional	MM (Main Module)	ST (Structures)	The structural subsystem shall be able to fit all the modules (Observation Module, Extraction Rover, Ore Retriever)
18 Functional	MM (Main Module)	TH (Thermal)	The thermal subsystem shall maintain the TBD operational temperature range of all subsystems
19 Functional	MM (Main Module)	TT&C (Telemetry, Tracking & Communication)	The communication subsystem shall receive commands from the ground station at the rate of TBD Mbps.
20 Functional	MM (Main Module)	PROP (Propulsion)	The propulsion system shall include redundant thrusters to ensure trajectory adjustments and orbit maneuvers in case of primary thruster failure
21 Functional	MM (Main Module)	PROP (Propulsion)	The propulsion system shall be capable of executing precise orbital insertions around the target MBC
22 Functional	MM (Main Module)	EP (Electrical Power)	The power subsystem shall include energy harvesting capabilities, such as solar panels
23 Functional	MM (Main Module)	OBCS (On-Board Computer & Software)	The OBCS subsystem shall support software updates to enhance mission capabilities, ensuring adaptability to evolving mission requirements.
24 Operational	MM (Main Module)	TH (Thermal)	The thermal subsystem shall feature passive thermal control measures to minimize thermal variations
25 Operational	MM (Main Module)	ST (Structures)	The structure subsystem shall deploy the Observation Module in its target orbit.
26 Operational	MM (Main Module)	EP (Electrical Power)	The power subsystem shall include a power storage system capable of storing TBD W to sustain spacecraft operations during eclipse periods.
27 Operational	MM (Main Module)	TT&C (Telemetry, Tracking & Communication)	The TT&C subsystem shall be designed to interface with multiple ground stations.
28 Operational	MM (Main Module)	ADCS (Attitude & Control)	The ADCS shall maintain a maximum attitude determination error of 0.05 degrees

Fig. 41. Subsystem Level Requirements

29	Functional	OM (Observation Module)	ADCS (Attitude & Control)	The ADCS subsystem shall de-tumble the module at TBD rate.
30	Functional	OM (Observation Module)	PL (Payload)	The system shall operate at TBD um wavelength.
31	Functional	OM (Observation Module)	ADCS (Attitude & Control)	The ADCS subsystem shall de-tumble the module at TBD rate.
32	Functional	OM (Observation Module)	OBCS (On-Board Computer & Software)	The OBCS subsystem shall implement machine learning algorithms for applying computer vision as part of the asteroid belt detection strategy.
33	Operational	OM (Observation Module)	ADCS (Attitude & Control)	The ADCS shall maintain a maximum attitude determination error of 0.05 degrees
34	Operational	OM (Observation Module)	TH (Thermal)	The thermal system shall maintain temperature variation of different subsystems to be within the operational range
35	Operational	OM (Observation Module)	TT&C (Telemetry, Tracking & Communication)	The TT&C subsystem shall be designed to interface with multiple ground stations.
36	Operational	OM (Observation Module)	EP (Electrical Power)	The power subsystem shall include a power storage system capable of storing TBD W to sustain spacecraft operations during eclipse periods.
37	Constraints	OR (Ore Retriever)	PL (Payload)	The payload subsystem shall provide TBD m3 of space to retrieve the target regolith quantity.
38	Functional	OR (Ore Retriever)	PL (Payload)	The payload subsystem shall carry the extracted resources back to the Main Module.
39	Functional	OR (Ore Retriever)	PROP (Propulsion)	The propulsion subsystem shall have the capability of launching from the surface of the MBC, preserving the scientific integrity of the regolith samples.
40	Functional	OR (Ore Retriever)	ST (Structures)	The structural subsystem shall be designed to withstand the mechanical loads associated with regolith sample containment and ascent from the asteroid surface
41	Operational	OR (Ore Retriever)	TH (Thermal)	The thermal subsystem shall implement insulation measures to protect the extracted resources from temperature variations during the return journey
42	Constraints			The mission shall be in final operating capability in TBD years.
43	Constraints			The total mass of the spacecraft shall be under 21 tons.
44	Constraints			The mission shall be executable using readily-available technologies.
45	Constraints			The mission shall comply with international space laws with respect to deorbiting.
46	Constraints			The total operational costs of the mission shall not exceed \$TBD.
47	Constraints			The total manufacturing costs of the mission shall not exceed \$TBD
48	Operational		ST (Structures)	The structure of all subsystems shall bear thermal loads within TBD temperature range.
49	Operational		TH (Thermal)	The thermal managementsubsystem shall maintain temperature gradient between any two points on the spacecraft to never exceed TBD degree.
50	Operational		EP (Electrical Power)	The power subsystems shall incorporate redundancy and fault-tolerant features.

Fig. 42. Subsystem Level Requirements Continued

B. ADCS Subsystem

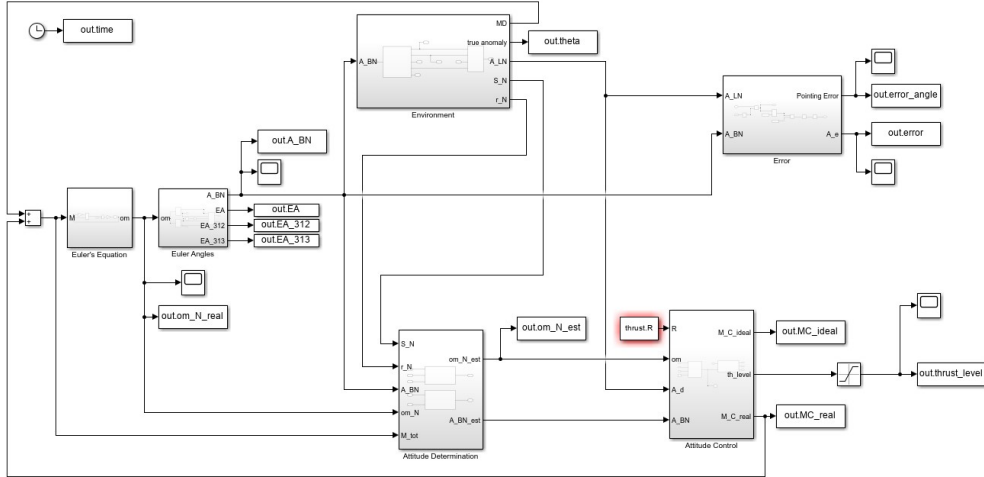


Fig. 43. Simulink Framework for pointing

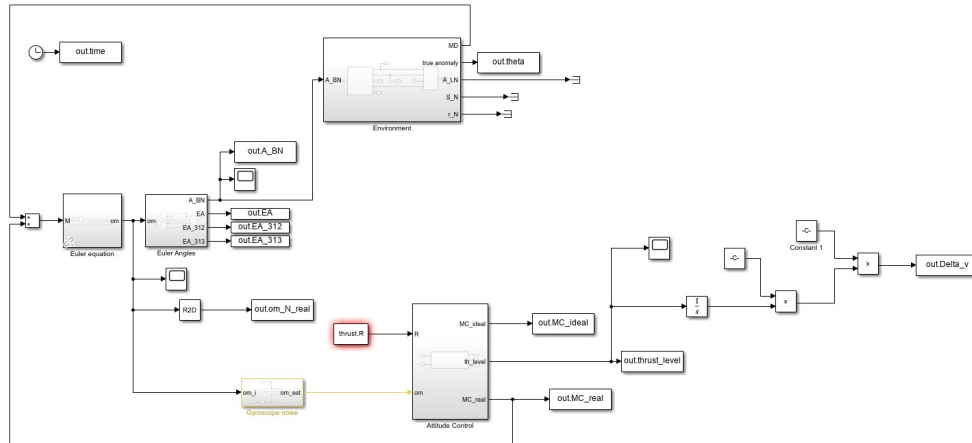


Fig. 44. Simulink Framework for detumbling

Solar Radiation Pressure [Nm]	9.4648e-09	9.5934e-09	8.1262e-09
Gravity Gradient [Nm]	7.7756e-10	2.0507e-11	6.5458e-12
Non-spherical shape [Nm]	2.5366e-13	2.0821e-15	4.2419e-16
Gravity of Didymoon [Nm]	3.9358e-11	1.5693e-13	4.6701e-14
Gravity of the Sun [Nm]	6.4152e-16	6.4402e-16	5.9834e-16
Gravity of the Earth [Nm]	2.1698e-21	2.0379e-21	2.0414e-21
Gravity of Jupiter [Nm]	7.2026e-21	6.935e-21	7.1067e-21
Total Torque [Nm]	1.02820e-08	9.61407e-09	8.13279e-09

Fig. 45. Reference disturbance torques in the asteroid belt at 1.8 AU for different satellite orbits

C. Power Subsystem

TABLE XXXIII
MOST COMMON SPACECRAFT POWER SOURCES COMPARISON

EPS Design Parameters	Solar Photovoltaic	Solar Thermal Dynamic	Radio-isotope	Nuclear Reactor	Fuel Cell
Power Range (kW)	0.2-300	5-300	0.2-10	5-300	0.2-500
Specific Power (W/kg)	25-200	9-15	5-20	2-40	2.75
Specific Cost (\$/W)	800-3,000	1,000-2,000	16K-200K	400K-700K	Insufficient Data
Hardness	Natural Radiation	Low-Medium	High	Very high	High
	Nuclear Threat	Medium	High	Very high	High
	Laser Threat	Medium	High	Very high	High
	Pellets	Low	Medium	Very high	Medium
Stability and Maneuverability	Low	Medium	High	High	High
Low-orbit Drag	High	High	Low	Medium (due to radiator)	Low
Degradation Over Life	Medium	Medium	Low	Low	Low
Storage Required for Solar Eclipse	Yes	Yes	No	No	No
Sensitivity to Sun Angle	Medium	High	None	None	None
Sensitivity to Spacecraft Shadowing	LOW (with bypass diodes)	High	None	None	None
Obstruction of Spacecraft Viewing	High	High	Low	Medium (due to radiator)	None
Fuel Availability	Unlimited	Unlimited	Very low	Very low	None
Safety Analysis Reporting	Minimal	Minimal	Routine	Extensive	Routine
IR Signature	Low	Medium	Medium	High	Medium

REFERENCES

- [1] Starship users guide, Mar 2020.
- [2] ITU Radiocommunication Assembly. Preferred frequency bands for deep-space research in the 1-40 ghz range. *ITU RECOMMENDATIONS*, Rec. ITU-R SA.1012.
- [3] Nicolas Biver, Dominique Bockelée-Morvan, Jacques Crovisier, Pierre Colom, Florence Henry, Raphaël Moreno, Gabriel Paubert, Didier Despois, and Dariusz C Lis. Chemical composition diversity among 24 comets observed at radio wavelengths. *Earth, Moon, and Planets*, 90:323–333, 2002.
- [4] D Bockelée-Morvan and N Biver. The composition of cometary ices. *Philosophical Transactions of the Royal Society A: Mathematical, Physical and Engineering Sciences*, 375(2097):20160252, 2017.
- [5] DHV Technology. Dhv technology products. Accessed: February 14, 2024.
- [6] T. Edwards. Liquid fuels and propellants for aerospace propulsion: 1903–2003. *Journal of Propulsion and Power*, 19(6):1089–1107, 2003.
- [7] Gianrico Filacchione, Olivier Groussin, Clémence Herny, David Kappel, Stefano Mottola, Nilda Oklay, Antoine Pommereh, Ian Wright, Zurine Yoldi, Mauro Ciarniello, et al. Comet 67p/cg nucleus composition and comparison to other comets. *Space science reviews*, 215:1–46, 2019.
- [8] O. Frota, B. Mellor, and M. Ford. Proposed Selection Criteria for Next Generation Liquid Propellants. In A. Wilson, editor, *ESA Special Publication*, volume 557 of *ESA Special Publication*, page 6.1, October 2004.
- [9] Erick Flores Garcia. Simulation of attitude and orbital disturbances acting on aspect satellite in the vicinity of the binary asteroid didymos.
- [10] David Jewitt, Jessica Agarwal, Harold Weaver, Max Mutchler, Jing Li, and Stephen Larson. Hubble space telescope observations of active asteroid 324p/la sagra. *The Astronomical Journal*, 152(3):77, Sep 2016.
- [11] Wiley J Larson and James R Wertz. Space mission analysis and design. *Torrance, CA (United States)*, 2004.
- [12] Wiley J. Larson and James R. Wertz. *Space mission analysis and design*. THE SPACE TECHNOLOGY LIBRARY. Kluwer Academic Publishers Microcosm Press, third edition, 2005.
- [13] Robert P Mueller, Rachel E Cox, Tom Ebert, Jonathan D Smith, Jason M Schuler, and Andrew J Nick. Regolith advanced surface systems operations robot (rassor). In *2013 IEEE Aerospace Conference*, pages 1–12. IEEE, 2013.
- [14] Robert P Mueller, Jonathan D Smith, Jason M Schuler, Andrew J Nick, Nathan J Gelino, Kurt W Leucht, Ivan I Townsend, and Adam G Dokos. Design of an excavation robot: regolith advanced surface systems operations robot (rassor) 2.0. In *ASCE Earth & Space Conference*, number STI NO. 25616, 2016.
- [15] David Reina. Spacecraft attitude dynamics and control.
- [16] Hans Rickman. Composition and physical properties of comets. In *Solar System Ices: Based on Reviews Presented at the International Symposium “Solar System Ices” held in Toulouse, France, on March 27–30, 1995*, pages 395–417. Springer, 1998.
- [17] Martin Rubin, Cécile Engrand, Colin Snodgrass, Paul Weissman, Kathrin Altwegg, Henner Busemann, Alessandro Morbidelli, and Michael Mumma. On the origin and evolution of the material in 67p/churyumov-gerasimenko. *Space science reviews*, 216(5):102, 2020.
- [18] satsearch. A-str and aa-str. Accessed: February 14, 2024.
- [19] satsearch. Cmg 40-60 s. Accessed: February 14, 2024.
- [20] satsearch. Ibeos b28-1100 satellite battery. Accessed: February 14, 2024.
- [21] satsearch. Smart sun sensor. Accessed: February 14, 2024.
- [22] satsearch. Spacecloud ix10-101a. Accessed: February 14, 2024.
- [23] satsearch. Starlight 1000 iru. Accessed: February 14, 2024.
- [24] J.Noyes J.Rouquet D.Stramaccioni) SCI-PRS (H.Fiebrich, D.Martinez Ripoll. Rosetta mission commissioning results review spacecraft performance report.
- [25] Dong K. Shin and California Institute of Technology. Frequency and channel assignments. *DSN*, 201(810–005), Sep 2020.
- [26] Fabio Caramelli Vittorio Bombelli, Ton Marée. Non-toxic liquid propellant selection method – a requirement-oriented approach. *41st AIAA/ASME/SAE/ASEE Joint Propulsion Conference & Exhibit*, 2005.
- [27] M. Wieling and J. A. F. van Oosterom. Development of a hydrogen peroxide/ethanol thruster for the advanced re-entry vehicle. *ESACCS 2019*, 2019.
- [28] Wikipedia contributors. International space station, Year. Accessed: Date.